(NASA-CR-137829) RADAR IMAGING FROM A SPINNING SPACECRAFT Final Report, 1 May - 1 Dec. 1975 (Environmental Research Inst. of Michigan) 92 p HC $5.00 CSCL 17I

N76-28452

Unclas
G3/32 47838

NASA CR-137829
ERIM 115200-2-F

Final Report

RADAR IMAGING FROM A SPINNING SPACECRAFT

ROBERT W. BAYMA
MOHAMED A. HIDAYET
Radar and Optics Division

MARCH 1976

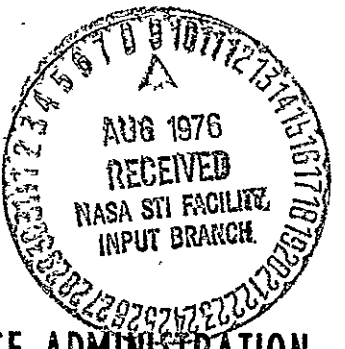

Prepared for
NATIONAL AERONAUTICS AND SPACE ADMINISTRATION

Ames Research Center
Moffett Field, California 24035
Contract No. NAS2-8860

ENVIRONMENTAL
RESEARCH INSTITUTE OF MICHIGAN
FORMERLY WILLOW RUN LABORATORIES THE UNIVERSITY OF MICHIGAN
BOX 618 • ANN ARBOR • MICHIGAN 48107

TECHNICAL REPORT STANDARD TITLE PAGE

1 Report No.	2. Government Accession No.	3. Recipient's Catalog No
NASA CR-137829		

4. Title and Subtitle	5. Report Date
RADAR IMAGING FROM A SPINNING SPACECRAFT	March 1976
	6. Performing Organization Code

7. Author(s)	8 Performing Organization Report No.
R. W. Bayma, M.A. Hidayet	ERIM 115200-2-F

9. Performing Organization Name and Address	10 Work Unit No
Radar and Optics Division Environmental Research Institute of Michigan, P.O. Box 618 Ann Arbor, Michigan 48107	11. Contract or Grant No NAS2-8860
	13. Type of Report and Period Covered Final report 1 May 75 - 1 Dec 75
12. Sponsoring Agency Name and Address Advanced Missions Office NASA Ames Research Center Moffet Field, California 24035	14. Sponsoring Agency Code

15 Supplementary Notes

16. Abstract

The objective of this study is to determine the feasibility of imaging the surface of Venus using a synthetic aperture radar in a spin-stabilized Pioneer class spacecraft operating in an eccentric orbit. Imaging radar fundamentals, constraints, power requirements and data processing considerations are reviewed in Sections 2 through 6. Additional effects due to operation from an elliptical orbit with a spinning spacecraft are covered in Sections 7 through 9. Recommended spin parameters are determined by simulations presented in Section 10. Extensions to include noncoherent integration and stereo coverage are briefly reviewed in Section 11.

The results of this study indicate that resolution on the order of 100 meters can be obtained from a 0.2 eccentricity orbit using a 2 meter antenna and reasonable transmitter power levels.

17. Key Words	18. Distribution Statement
Imaging radar Synthetic aperture radar Venus orbital imaging radar	

19. Security Classif. (of this report)	20. Security Classif. (of this page)	21. No. of Pages	22. Price
Unclassified	Unclassified	92	

PREFACE

This report was prepared by the Radar and Optics Division of the Environmental Research Institute of Michigan (ERIM), Ann Arbor, Michigan, under contract No. NAS2-8860 with NASA Ames Research Center, Moffett Field, California. This report describes work performed between 1 May 1975 and 1 December 1975. The effort was monitored by Larry E. Edsinger, Advanced Mission Office, NASA Ames Research Center. The ERIM number for this report is 115200-2-F.

The Principal Investigator for this study is Robert W. Bayma. Sections 1 - 9 and 11 of this report were written by R. W. Bayma. Section 10 was written by M. A. Hidayet. Additional contributions to this study were made by C. C. Aleksoff. The authors are also grateful to Robert C. Heimiller for his constructive review of the draft version of this report.

SUMMARY

Recent NASA studies have been conducted to determine the feasibility of imaging the Venusian surface using an orbiting synthetic aperture radar (SAR).

The earliest studies on orbital radar imaging have emphasized mapping from a circular orbit. This method simplifies the radar system since processing parameters remain constant. However, because of spacecraft propulsion constraints, and data transfer considerations, it can be advantageous to operate from an elliptical orbit.

Significant problems associated with SAR imaging from a highly elliptical orbit include the compensation for a large, varying, time delay and radial-velocity-induced Doppler frequency shift; transmit-receive interlacing over a large change in slant range; and large change in azimuth focal parameters. However, these problems are reduced by using a batch processing mode.

Previous studies utilized a three-axis stabilized spacecraft. A planned Pioneer Venus Orbiter mission uses a less expensive spin-stabilized spacecraft for altimetry and coarse resolution imaging. The purpose of this study is to determine the feasibility of obtaining improved resolution on the order of 100 meters from a spin-stabilized Pioneer class spacecraft. This report begins with a review of imaging radar fundamentals, and proceeds to discuss restrictions encountered with a spinning spacecraft.

For coherent radars, range resolution is determined by RF bandwidth, and azimuth resolution is determined by the coherent integration time or synthetic aperture length. The coherent integration time can correspond to a single pulse, or to the total interval covered by a number of pulses processed

for unfocused or focused synthetic aperture radars. In the later case, the total synthetic aperture length is limited by the target illumination time, which is equal to the transit time through the real antenna beam for a 3-axis stabilized spacecraft, or is equal to the time-on-target during a scan for a spin-stabilized spacecraft.

When operating from an elliptical orbit with a limited antenna aperture, delay-Doppler ambiguity constraints limit coverage at the higher altitudes and shallow grazing angles. Power requirements may also limit coverage at the higher altitudes.

Because the data is collected in bursts, batch mode processing will be required. On-board processing will be limited to Doppler tracking, which will be required to compensate for the change in instantaneous Doppler center frequency due to antenna scanning and spacecraft radial velocity, and PRF buffering. For 6 bit quantization, the telemetry data rate is approximately 180 kbps. The PRF buffer storage is 3 kbits and the total buffer storage for a spin cycle is 3 Mbits.

Azimuth correlation would be done with a ground based digital processor. Range pulse compression would be done either in the spacecraft or with the ground processor.

Performance results are given for three principle spin axis orientations: 1) in the orbital plane, 2) normal to the orbital plane, and 3) a third general orientation. A computer program was developed which calculates the mapping parameters, the power requirements, and the surface longitude

and latitude of the target point for a given circular antenna aperture diameter, antenna mounting angle and a spin vector. A modified version calculates the same parameters when the angular orientation of the antenna is continuously directed toward the direction of maximum grazing angle. Since the optimal mapping parameters and minimum power requirement occur at the direction of maximum grazing angle, the modified version generates the envelope for the curves generated during individual spin cycles.

The results obtained from this study indicate that by placing the spin axis normal to the orbital plane and the antenna mounting angle such that the boresight is 10 to 15 degrees off nadir, complete planet coverage at 30 to 160 meter azimuth resolution is attainable. The average operating transmitter power required for a SNR of 10 dB is 10 to 200 watts during a nominal 120 msec mapping interval once per spin cycle. The average power over a 12 second spin cycle is 0.1 to 2 watts.

The results of this study demonstrate mission feasibility. A baseline design study is recommended to optimize the selection of orbital and radar parameters and to investigate processing algorithms in detail.

CONTENTS

FIGURES

GLOSSARY

A	antenna area
$a(\theta)$	two-way antenna voltage gain
B	Rf bandwidth
B	Doppler frequency to first null of antenna azimuth pattern
B_a	azimuth Doppler bandwidth
B_D	Doppler filter bandwidth
c	velocity of propagation
C_A	azimuth compression ratio
C_R	range compression ratio
d	antenna diameter
d_a	antenna azimuth aperture dimension
d_e	antenna elevation aperture dimension
e	orbit eccentricity
f_D	Doppler frequency
h	radar altitude
k	Boltzmann constant
L	RF and propagation losses
L_A	synthetic aperture length
N_A	number of pulses per synthetic aperture interval
N_B	Buffer storage for a spin cycle
N_{PRF}	Buffer storage for pulse repetition period
P	average transmitter power
q	quantized word size
R	slant range

R_{AVE}	average video data rate
R_B	buffered video data rate
R_{min}	minimum video data rate
R_V	raw video data rate
$s(\theta)$	processed signal
S	spacecraft spin rate
SNR	signal-to-noise ratio
T	coded pulse length
T	Delay to first null of antenna elevation pattern
T	Length of video return
T_A	coherent integration time
T_M	mapping time interval
TB	time-bandwidth product
T_e	effective receiver temperature
V	radar velocity
V_N	radar velocity component normal to the line of sight
$\vec{V}_P$	radar velocity vector at periapsis
W	azimuth patch length
x	radar position along synthetic array
x_n	position of radar at n-th pulse
β_a	azimuth beamwidth
β_e	elevation beamwidth
Δf_D	Doppler bandwidth
ΔR	slant range interval
ΔT	uncoded pulse length

$\Delta T'$	compressed pulse length
Δx	azimuth spatial sampling interval
$\Delta\theta$	angular azimuth resolution
η	antenna aperture efficiency
ϕ_n	received phase of n-th pulse
ϕ_s	angle between the projection of the spin vector on the orbit plane and the radial position of the spacecraft at periapsis
θ_A	angular synthetic aperture interval
θ_m	angle between antenna boresight and spin axis
θ_P	angle between velocity vector and antenna boresight
θ_s	angle between spin vector and orbit plane
θ_T	angle between velocity vector and target line-of-sight
λ	RF wavelength
ρ_a	azimuth resolution
ρ_g	ground resolution
ρ_o	azimuth resolution for a non-spinning spacecraft
ρ_r	slant range resolution
σ_o	backscatter coefficient
ψ	grazing angle
$\vec{\Omega}_P$	angular velocity of the antenna
$\vec{\Omega}_T$	angular velocity of the target line-of-sight

1
INTRODUCTION

Recent achievements in planetary exploration have included the collection of fine resolution visual imagery of the planets Mars and Mercury from various Mariner spacecraft. However, the cloud covered surface of the Earth's nearest neighbor planet, Venus, defies visual imaging systems.

Earth-based radar astronomy has permitted us to determine the rotation rate of Venus, and has also yielded coarse resolution radar reflectivity maps of the planet surface. Recent upgrading of the Arecibo radar site is expected to permit resolutions of 1 to 2 km near the subradar point at inferior conjunction. However, the Mercury imaging missions have demonstrated that surface resolutions of 100 m or less are required to identify important geological features. Hence, recent NASA studies [1-4] have been conducted to determine the feasibility of imaging the Venusian surface using an orbiting synthetic aperture radar (SAR).

The JPL studies [2] on orbital imaging radar have emphasized mapping from a circular orbit. This method simplifies the radar system since processing parameters remain constant. However, a circular orbit is not necessary, since, unlike visual imaging systems, SAR resolution can be made independent of range. In addition, due to spacecraft propulsion constraints and data transfer considerations, it can be advantageous to operate from an elliptical orbit.

Significant problems associated with SAR imaging from a highly elliptical orbit include the compensation for a large varying radial-velocity-induced Doppler frequency shift; transmit-

receive interlacing over a large change in slant range; and large change in azimuth focal parameters. The Martin-Marietta-ERIM study [4] demonstrated that these problems could be easily handled by using a batch processing mode, since PRF, range gating and other radar parameters can be changed at discrete intervals as required.

Previous studies [1-4] utilized a three-axis stabilized spacecraft. A planned Pioneer Venus Orbiter mission [5] uses a less expensive spin-stabilized spacecraft for altimetry and coarse resolution imaging. The purpose of this study is to determine the feasibility of obtaining improved resolution on the order of 100 meters from a spin-stabilized Pioneer class spacecraft.

Nominal parameters used in this study are listed below:

orbit eccentricity:	≥ 0.2
periapsis altitude:	500 km
maximum antenna diameter:	3 meters
spin rate:	2 to 30 rpm
wavelength:	10 cm

Orbit and spacecraft constraints were given by the Advanced Missions Office, NASA Ames Research Center. The wavelength was the same used in previous Martin-Marietta-ERIM studies [3,4].

This report begins with a review of imaging radar fundamentals, and proceeds through a discussion of restrictions encountered with a spinning spacecraft. Performance results are given for three principle spin axis orientations: 1) in the orbital plane, 2) normal to the orbital plane and 3) a third general orientation.

2
IMAGING RADAR FUNDAMENTALS

2.1 INTRODUCTION

The principal imaging radar system is the sidelooking airborne radar (SLAR) which obtains along-beam or range resolution by measuring time delay between returns from image elements; and obtains cross-beam or azimuth resolution by using a real aperture (narrow beam) antenna, or a synthetic aperture (Doppler signal processing) technique. Most SLAR systems operate at broadside in which the antenna is directed normal to the radar velocity vector, and consequently, range resolution is cross-track and azimuth resolution is along-track. This is not a fundamental requirement, since these radars can attain the same resolution at any squint angle that is not coincident with the velocity vector.

A second class of imaging radars is the microwave hologram radar (MHR) which attains cross-track resolution using real aperture phased array techniques, and along track resolution using synthetic array techniques. These radars can image along and to both sides of the ground track using an unmodulated (CW) signal. However, in order to obtain fine cross-track resolution, the radar must be operated at low altitude, or at moderate altitudes using the shortest possible wavelength and largest possible antenna aperture. Such a system would not be practical for the Venus mapping mission, but is listed here for completeness. Additional discussions on MHR systems are given in References [6-7] .

In the following two sub-sections, range and azimuth resolution for imaging radars are discussed from the point of view of temporal signal processing and filtering theory. In Section 3 of this report, SAR azimuth resolution is further considered from the point of view of linear antenna array theory.

2.2 RANGE RESOLUTION

The nominal slant range resolution attainable using an uncoded rectangular pulse of length ΔT is

$$\rho_r = \frac{c}{2} \Delta T \tag{1}$$

where c is the velocity of propagation. The required RF bandwidth is

$$B = \frac{1}{\Delta T} \tag{2}$$

The output signal-to-noise ratio (SNR) of any radar system is proportional to the energy in the radar pulse. Consequently, the required peak transmitted power for a specified signal-to-noise ratio is inversely proportional to pulse length. For a fine resolution radar, the peak power requirements become excessive if a simple rectangular pulse is used. Hence, a longer coded pulse of length T and bandwidth B is used. By processing the received signal with the appropriate matched filter, the pulse can be compressed to an effective length of

$$\Delta T' = \frac{1}{B} \tag{3}$$

Then the effective slant range resolution is

$$\rho_r = \frac{c}{2B} \tag{4}$$

The pulse compression ratio is

$$C_R = \frac{T}{\Delta T'} = TB \tag{5}$$

The detailed structure of the compressed waveform depends on both the waveform modulation and Doppler shift of the return. This structure is usually given by the radar ambiguity function which describes the interfering power from targets at other ranges and Doppler shifts which are present at the output of the filter matched to a specified range and Doppler shift.

The most common types of coded waveforms used for pulse compression are linear FM (chirp) signals and binary phase codes. These signals can be generated and compressed both actively and passively at RF, IF or video frequencies.

Slant range resolution is the projection of the ground range resolution cell normal to the line of sight. Thus

$$\rho_r = \rho_g \cos \psi \tag{6}$$

where ψ is the grazing angle. Substituting Eq. (4) in (6), the ground resolution can be expressed in terms of RF bandwidth and grazing angle as

$$\rho_g = \frac{c}{2B} \sec \psi \tag{7}$$

2.3 AZIMUTH RESOLUTION

Azimuth resolution is defined in the mapping plane determined by the radar velocity vector and the radar line-of-sight, and is measured normal to the radar line of sight. Ground resolution is determined by the projection of the azimuth resolution element along lines of constant Doppler frequency, which are cones concentric with the radar velocity vector.

2.3.1 NONCOHERENT IMAGING RADAR

In a noncoherent SLAR, the phase of the returned pulse is not available, or is not used. In such a system, the azimuth resolution is determined by the real aperture beamwidth.

In this case

$$\rho_a = R\beta_a$$

$$\simeq R \frac{\lambda}{d_a} \qquad (8)$$

where β_a is the azimuth beamwidth and d_a is the azimuth aperture dimension. Operational radars of this type are the Motorola AN/APS-94 and the Westinghouse AN/APQ-97 imaging radars.

2.3.2 SINGLE PULSE DOPPLER BEAM SHARPENING

For the case of single pulse Doppler beam sharpening, such as proposed for the planned Pioneer Venus Orbiter Radar Mapper [5], the radar is required to be coherent over the length of the transmitted pulse. The spectrum of the returned pulse is broadened by the Doppler spread of the illuminated terrain. Azimuth resolution (Doppler beam sharpening) is improved by filtering the returned signal prior to detection. The azimuth resolution is determined by the bandwidth of the Doppler filter.

The instantaneous Doppler frequency of a target at an angle θ from the vehicle velocity vector is

$$f_D = \frac{2V}{\lambda} \cos \theta \qquad (9)$$

For small angles, the Doppler bandwidth is given by

$$\Delta f_D = \frac{2V_N}{\lambda} \Delta\theta \tag{10}$$

where

$$V_N = V \sin \theta \tag{11}$$

is the radar velocity normal to the target line-of-sight. The Doppler spread from homogeneous terrain for a radar with azimuth beamwidth β_a is then

$$B_a = \frac{2V_N}{\lambda} \beta_a \tag{12}$$

By processing the returned pulse with a Doppler filter of bandwidth B_D, with $B_D < B_a$, the angular resolution can be improved to

$$\Delta\theta = \frac{\lambda}{2V_N} B_D \tag{13}$$

The minimum attainable Doppler resolution is equal to the reciprocal of the pulse length T. Then

$$\Delta\theta \geq \frac{\lambda}{2V_N T} \tag{14}$$

From Eqs. (13) or (14), the azimuth resolution is

$$\rho_a = \frac{R\lambda}{2V_N} B_D$$

$$\geq \frac{R\lambda}{2V_N T} \tag{15}$$

Note that $V_N T$ is the distance the radar travels normal to the line-of-sight during the Doppler processing time.

In order to improve the azimuth resolution by Doppler filtering, the pulse length must satisfy the inequality

$$V_N T > d_a/2 \tag{16}$$

that is, the "effective" aperture must be greater than half the real aperture.

If an uncoded pulse is used, the slant range resolution is

$$\rho_r = \frac{cT}{2} \tag{17}$$

Then

$$\rho_a \geq \frac{R\lambda c}{4\rho_r V_N}$$

and the best attainable areal resolution is

$$\rho_a \rho_g = \rho_a \rho_r \sec \psi$$

$$= \frac{R\lambda \, c \sec \psi}{4V_N} \tag{19}$$

For the nominal parameters considered in this study, the attainable resolution is on the order of 50 km by 50 km.

By using a parallel bank of Doppler filters and a sufficiently long pulse, the real azimuth beam can be subdivided into several resolvable synthetic beams, and a coarse resolution radar image can be generated from the return of a single pulse. However, from Eq. (19), we note that resolution

is proportional to $R\lambda/V_N$, hence, this type of imaging is attractive only for short range, short wave-length, high velocity radars.

2.3.3 COHERENT PULSED DOPPLER RADARS

In a coherent pulsed Doppler radar, the radar is coherent over several transmissions. The phase of the returned pulse is measured with respect to that of a stable oscillator. In this manner, successive returns may be processed coherently in order to attain finer Doppler resolution. A synthetic aperture radar is a member of this class.

By interpreting N successive pulses as a single coded transmitted signal, the azimuth resolution can be determined in the same manner as the noncoherent imaging radar. If T_A is the time interval for N_A pulses,

$$T_A = \frac{N_A}{PRF} \tag{20}$$

then the attainable azimuth resolution is

$$\rho_a = \frac{R\lambda}{2T_A V_N} \tag{21}$$

Now, because the angle to a target changes with time, the returned signal does not remain in the pass-band of the Doppler filter indefinitely; hence, the integration time

T_A is limited. The change in Doppler frequency with time is

$$\Delta f_D = \frac{2}{\lambda} \frac{V_N^2 t}{R} \tag{22}$$

where t is measured from the center of the aperture. Then at $t = \pm T_A/2$, the Doppler frequency shift should be no more than half the Doppler resolution attainable with a filter integration length equal to T_A. This requires

$$\frac{2V_N^2}{R\lambda} \frac{T_A}{2} \leq \frac{1}{2T_A} \tag{23}$$

or

$$T_A \leq \frac{1}{V_N} \sqrt{\frac{R\lambda}{2}} \tag{24}$$

Then

$$\rho_a \geq \frac{R\lambda}{2T_A V_N} = \sqrt{\frac{R\lambda}{2}} \tag{25}$$

A system of this type is an unfocused synthetic aperture radar. Note that resolution is independent of beamwidth and radar velocity, and is proportional to the square root of range.

The integration time can be extended by compensating for the change in Doppler frequency during the data processing interval. This means that the received signal must be mixed with a linearly changing reference frequency which matches the Doppler rate. Then the coherent integration interval is equal to the length of time the antenna illuminates the target. This is given by

$$T_A = \frac{R}{V_N}\beta_a$$

$$= \frac{R}{V_N}\frac{\lambda}{d_a} \qquad (26)$$

Then the attainable resolution is

$$\rho_A \geq \frac{R\lambda}{2T_A V_N} = \frac{d_a}{2} \qquad (27)$$

which is the limiting resolution for a fixed antenna SAR.

2.4 SYNTHETIC APERTURE RADAR

A synthetic aperture radar (SAR) is a coherent pulsed Doppler SLAR which employs a relatively small antenna to

synthesize, in effect, an aperture many times larger than the actual antenna by utilizing the relative motion of the transport vehicle. The radar echo is stored and processed by a computer (digital or optical) to produce a detailed strip map of the terrain. The azimuth resolution can be made independent of range by "focusing" simultaneously at all ranges in the processing.

Basic signal processing concepts are identical to those discussed in the previous section. A different approach will be presented in Section 3.

Historically, most SAR's have operated in a non-real-time mode in which the return is coherently recorded as a two-dimensional signal history on photographic film and then processed in a coherent optical processor. Recent advances in digital circuit technology now permit real-time processing for moderate scene sizes and resolutions. Whenever complete on-board processing is not feasible, such as aboard a light-weight spacecraft, digital preprocessing techniques can be used to minimize data storage or data link bandwidth requirements for the non-redundant video data.

3
SYNTHETIC APERTURE RADAR RESOLUTION THEORY

3.1 INTRODUCTION

In the previous section, an expression for the azimuth resolution of a SAR was given based on Doppler filtering of the coherent returned signal history. In this section, a brief derivation of the achievable resolution will be given in terms of linear antenna array theory.

3.2 ANGULAR RESOLUTION OF A SYNTHETIC ARRAY

Let x denote the position of the radar along the synthetic array shown in Figure 3-1. Let

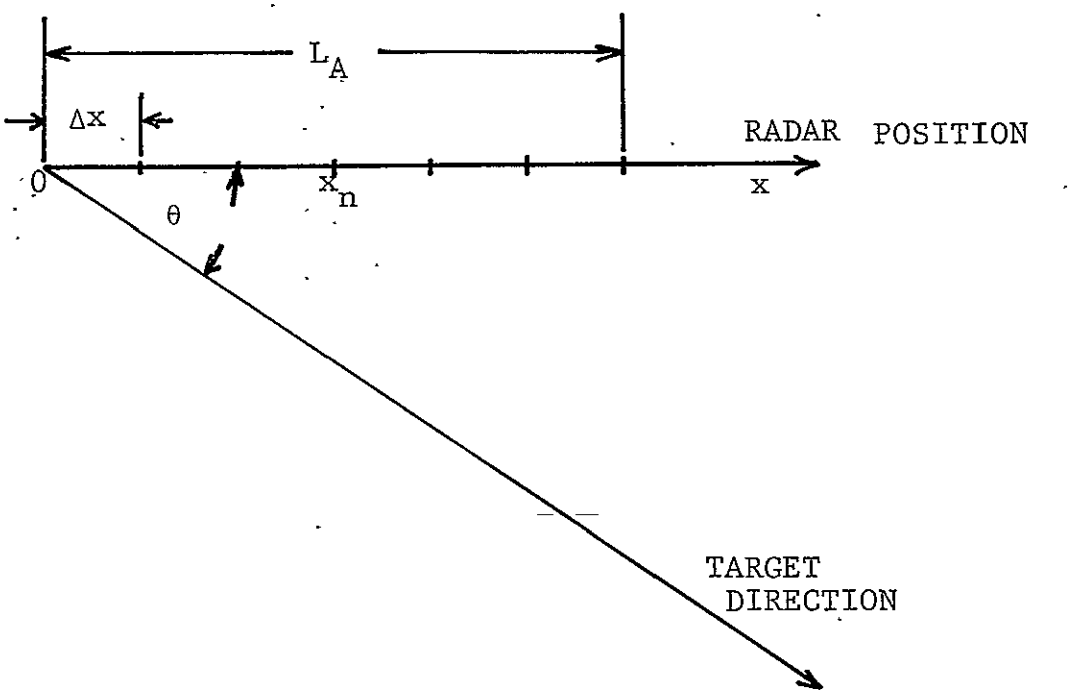

Figure 3-1: Synthetic Array Geometry

where the two-way phase

$$\phi_n = -4\pi \frac{n\Delta x}{\lambda} \cos \theta \tag{30}$$

is measured with respect to the phase of the first return, and the amplitude $a(\theta)$ is proportional to the two-way voltage gain of the radar antenna in the direction θ.

Then, for a uniformly weighted synthetic array, the response in the direction θ_o is proportional to

$$\left| a(\theta) \frac{1}{N} \sum_{n=0}^{N-1} \exp \left\{ -4\pi i \, n \frac{\Delta x}{\lambda} (\cos \theta - \cos \theta_o) \right\} \right|^2$$

$$= |a(\theta)|^2 \frac{\sin^2 \left[2\pi N \frac{\Delta x}{\lambda} (\cos \theta - \cos \theta_o) \right]}{N^2 \sin^2 \left[2\pi \frac{\Delta x}{\lambda} (\cos \theta - \cos \theta_o) \right]}$$

$$\simeq |a(\theta)|^2 \frac{\sin^2 \left[2\pi \frac{L_A \sin \theta_o}{\lambda} (\theta - \theta_o) \right]}{N^2 \sin^2 \left[2\pi \frac{\Delta x \sin \theta_o}{\lambda} (\theta - \theta_o) \right]} \tag{31}$$

The angular resolution to the first null of the synthetic pattern is

$$\Delta\theta = \frac{\lambda}{2L_A \sin \theta_o} \tag{32}$$

and the corresponding azimuth resolution at slant range R is

$$\rho_a = R\Delta\theta$$

$$= \frac{R\lambda}{2L_A \sin \theta_o} \tag{33}$$

which is identical to Eq. (21) if we make the substitution

$$L_A \sin \theta_o = V_N T_A \tag{34}$$

If $R >> L_A$, the angular synthetic aperture interval is given by

$$\theta_A = \frac{L_A \sin \theta_o}{R} \tag{35}$$

in which θ_A is the total angular change during processing. Then the expression for azimuth resolution is conveniently written as

$$\rho_a = \frac{\lambda}{2\theta_A} , \quad \theta_A << 1 \tag{36}$$

3.3 UNFOCUSED SYNTHETIC APERTURE

Equations (28) through (31) strictly apply only if the target is in the far field of the synthetic pattern. The limiting aperture length is usually defined by the maximum length over which the two-way quadratic phase error is less than $\pi/2$. The maximum array length is then

$$L_A \sin \theta_o = \sqrt{R\lambda} \tag{37}$$

Then the azimuth resolution for an unfocused synthetic array is bounded by

$$\rho_a \geq \frac{R\lambda}{2L_A \sin \theta_o} = \frac{\sqrt{R\lambda}}{2} \tag{38}$$

which differs from Eq. (25) by a factor of 0.7. (Equation (25) is more conservative in that it allows a maximum quadratic phase error of $\pi/4$.)

3.4 FOCUSED SYNTHETIC APERTURE

If finer resolution is required, the synthetic aperture length must be increased beyond that given by Eq. (37). Then the quadratic (and higher) phase terms must be matched over the processing aperture. It can be shown that the two-way change in phase over the synthetic array is approximately

$$\phi(x) = -\frac{4\pi}{\lambda}\left(x\cos\theta - \frac{x^2}{2R}\sin^2\theta\right) \qquad (39)$$

where θ is the angle to the target and R is the range. Unfocused processing compensates for the first term in Eq. (39). Focused processing compensates for the first and second. The limiting aperture length is determined by the real antenna illumination and is nominally

$$L_A \sin\theta = R\beta_a = \frac{R\lambda}{d_a} \qquad (40)$$

The limiting resolution is $d_a/2$ or $\lambda/(2\beta_a)$ which can be obtained by substitution of Eq. (40) into (33). This result is identical to (27).

A measure of the azimuth processing complexity is the azimuth compression ratio which is

$$C_A = \frac{L_A \sin \theta}{\rho_a}$$

$$= \frac{R\lambda}{2\rho_a^2} \qquad (41)$$

It can be shown that the memory requirement for digital processing of the synthetic array data is proportional to C_A. For an unfocused SAR system, the best resolution is achieved for $C_A = 2$ if equations (37) and (38) are used to define array length and resolution.

4
SAR AMBIGUITY CONSTRAINTS

4.1 INTRODUCTION

The pulse repetition frequency (PRF) of a SAR must be high enough to sample the received Doppler spectrum, and simultaneously, be low enough to prevent confusion with second-time-around (STA) echoes. For a given PRF, squint angle and target grazing angle, the ambiguity constraints lead to antenna beamwidth constraints and corresponding target coverage constraints.

4.2 AZIMUTH APERTURE CONSTRAINT

The Doppler bandwidth to the first null corresponding to a uniformly illuminated rectangular aperture is

$$B = \frac{2V_N}{d_a} \tag{42}$$

where V_N is the radar velocity normal to the line-of-sight, and d_a is the azimuth aperture length. It is shown in Ref. [8] that azimuth ambiguities are negligible if the two way antenna gain is down by at least 16 dB at the Doppler cone angle corresponding to the PRF. Hence*

$$\begin{aligned} PRF &\geq 1.356\ B \\ &\geq 2.712\ \frac{V_N}{d_a} \end{aligned} \tag{43}$$

*Complex sampling, or range offset video is assumed, otherwise, the PRF constraint must be doubled.

This leads to a nominal azimuth aperture constraint of

$$d_a \geq \frac{2.712\ V_N}{PRF} \tag{44}$$

4.3 ELEVATION BEAMWIDTH CONSTRAINT

The two-way echo delay to the first null over the illuminated swath is given by

$$T = \frac{2R\lambda}{c\ d_e\ \tan\ \psi} \tag{45}$$

where d_e is the elevation aperture height, and ψ is the grazing angle at the target patch. To eliminate STA echo ambiguities, the PRF must satisfy the constraint [8].

$$PRF \leq \frac{1}{1.356\ T}$$

$$\leq \frac{c\ d_e\ \tan\ \psi}{2.712\ R\lambda} \tag{46}$$

This requires an elevation aperture constraint of

$$d_e \geq \frac{2.712\ R\lambda}{c \tan \psi} PRF \tag{47}$$

4.4 PRF AND TIME BANDWIDTH CONSTRAINT

Combining Eqs. (43) and (46) we get the PRF constraint

$$1.356\ B \leq PRF \leq \frac{1}{1.356\ T} \tag{48}$$

In order to satisfy Eq. (48), the time-bandwidth product (TB) of the illuminated swath must satisfy the constraint

$$TB \leq (1.356)^{-2} = 0.54 \tag{49}$$

If TB > 1, then coherent pulse Doppler imaging, or even range pulse compression cannot be used due to the self clutter induced by Doppler ambiguities. In this case, simple single pulse radar imaging is required with the resulting resolution constraint given in Eq. (19).

If TB < 1 then synthetic array techniques can be used. To realize a signal-to-ambiguity ratio of about 20 dB requires that TB < 0.54. For larger values of TB, the self clutter level due to delay-Doppler ambiguities will increase at the edge of the scene, gradually moving toward the center as TB → 1. Thus, the system essentially fails gracefully.

5
SAR POWER REQUIREMENTS

Signal-to-noise ratio (SNR) is the ratio of the average clutter energy to average radar noise energy in an image resolution cell. One convenient formulation for the case of a limited antenna aperture is

$$SNR = \frac{P\,\eta^2\,A^2\,c\,\sigma_o}{16\pi\,kT_eBL\,R^3\,\lambda\,V_N\cos\psi}\,,\quad 0 < \psi < \pi/2 \qquad (50)$$

where

P = average transmitted power
η = antenna aperture efficiency
A = antenna area
c = velocity of propagation
σ_o = surface backscatter coefficient per unit area
k = Boltzman's constant
T_e = effective receiver temperature
B = RF bandwidth
L = RF and propagation losses
R = slant range
λ = radar wavelength
V_N = radar velocity normal to the line of sight
ψ = grazing angle at the surface

Note that the SNR is independent of azimuth resolution. This is due to the fact that the image clutter return is noise-like, and as the azimuth integration time is increased

in order to improve azimuth resolution, signal and noise energy both increase at the same rate.

For this study, the following fixed parameter values were assumed:

$T_e = 700^{\circ}K$ $\quad\quad$ $\lambda = 10$ cm

$\eta = 0.85$

$B = 3$ MHz

$L = 10$ dB

The model for the surface backscatter coefficient as a function of grazing angle was taken from Ref [5]:

$$\sigma_o = \frac{0.0133 \sin \psi}{(\cos \psi + 0.1 \sin \psi)^3} \tag{51}$$

and is plotted in Figure 5-1.

According to eqs. (50) and (51), SNR is a function of RF bandwidth and grazing angle. When mapping near nadir, planet curvature can be neglected, and slant range can be approximated by

$$R = \frac{h}{\sin \psi} \tag{52}$$

where h is the radar altitude. Then from Eqs. (50-52), SNR can be expressed in terms of velocity, surface grazing angle and bandwidth as

$$SNR = \frac{K \sin^3\psi}{V_N} \cdot \frac{c}{2B \cos\psi} \cdot \frac{0.0133 . \sin\psi}{(\cos\psi + 0.1 \sin\psi)^3}, \quad \psi < \frac{\pi}{2} \tag{53}$$

where K contains all other constant terms of Eq. (50). The second factor in Eq. (53) is the ground range resolution ρ_g given by Eq. (7), and is plotted in Figure 5-2 for $B = 3$ MHz. (Note that Eqs. (50) and (53) are invalid at 90° grazing angle for which the ground resolution approaches the limit, $2\sqrt{hc/B}$.)

From Eq. (53), we then observe that for a fixed bandwidth, SNR is maximized when operating at the largest possible grazing angle. However, from Figure 5.2, we note that ground resolution degrades rapidly at large grazing angles. In addition, radar layover is emphasized at steep grazing angles when imaging terrain features have significant elevation relief. For the study, grazing angles were therefore kept to 80° or less.

By increasing the RF bandwidth at large grazing angles, ground resolution can be held constant. However, in this case, the loss in SNR due to increased noise bandwidth is more than overcome by the increased backscatter coefficient, and SNR is still maximized when operating at maximum grazing angle.

Previous Venus Mapper studies [2-4] have emphasized mapping at steep grazing angles (on the order of 80°),

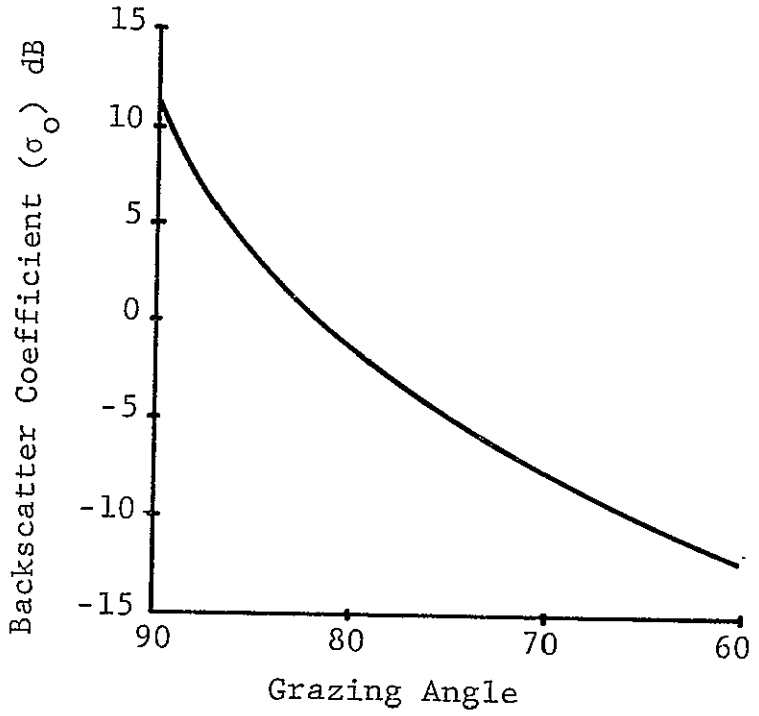

Figure 5-1. Terrain Backscatter Coefficient

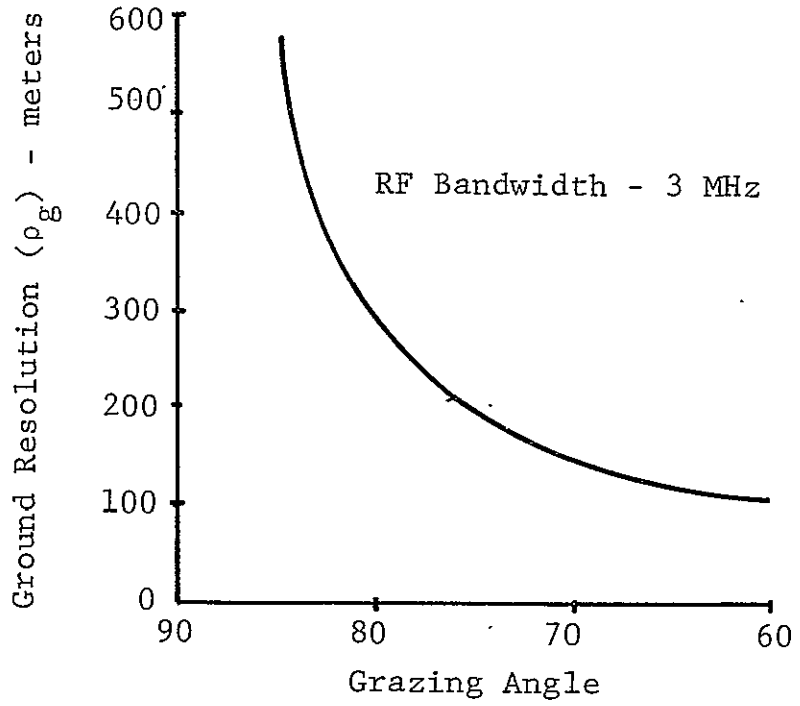

Figure 5-2. Ground Resolution

primarily due to SNR considerations based on the backscatter model given in Eq. (51). However, no significant amount of radar imagery is available at steep grazing angles to assist in evaluating its utility. Verification of utility as well as the backscatter model at steep grazing angles is required to add confidence to mission feasibility.

6
SAR DATA PROCESSING

6.1 INTRODUCTION

In this section we will briefly describe two approaches to SAR azimuth data processing. More detailed descriptions are available in Refs. [9 and 10] . It will be assumed that range compression, if required, is done first at RF, IF, or video frequencies. The radar azimuth data is sampled at the PRF rate. It will be assumed that the data is also sampled in range. Processing algorithms will be described for a single range bin. Similar processing will be required simultaneously for all range bins in the image, where, in general, processing parameters are a slowly varying function of range.

6.2 CONTINUOUS PROCESSING

In the continuous or line-by-line processing mode, a single azimuth image element is generated at each range interval each time the radar moves a distance equal to the azimuth resolution cell width. This is illustrated in Figure 6-1. In this mode, the required radar spatial sampling interval is equal to the desired azimuth resolution cell width. The minimum number of azimuth samples required is equal to the azimuth compression ratio given by Eq. (41). For focused SAR processing, the azimuth compression ratio is greater than 1, hence the synthetic aperture length is greater than the resolution cell size.

If the PRF corresponds to a finer azimuth sampling rate than required, then the data is presummed or prefiltered before azimuth compression. Presumming removes excess Doppler information from the azimuth signal, which then permits resampling at the lower rate.

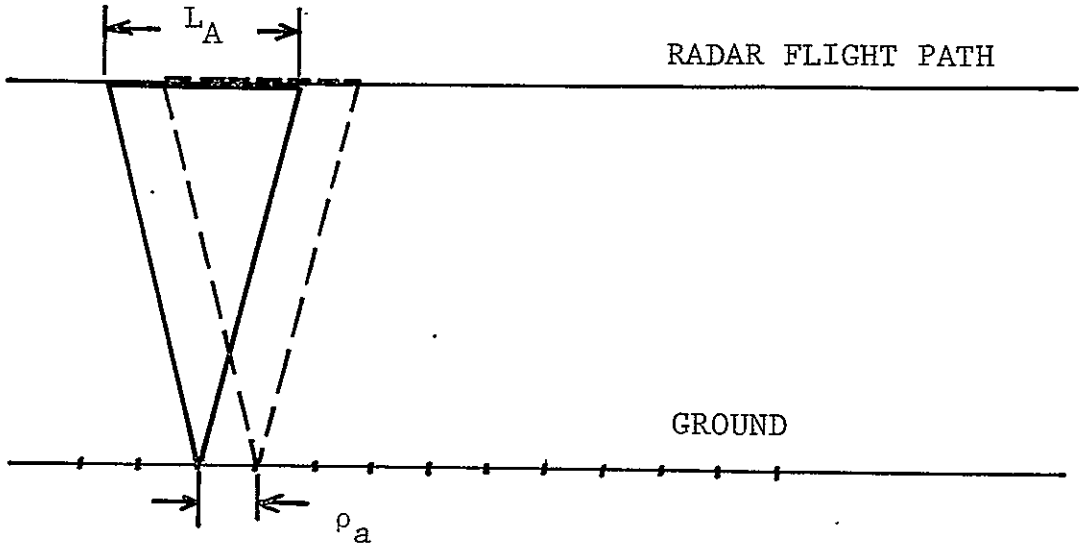

Figure 6-1. Continuous Processing

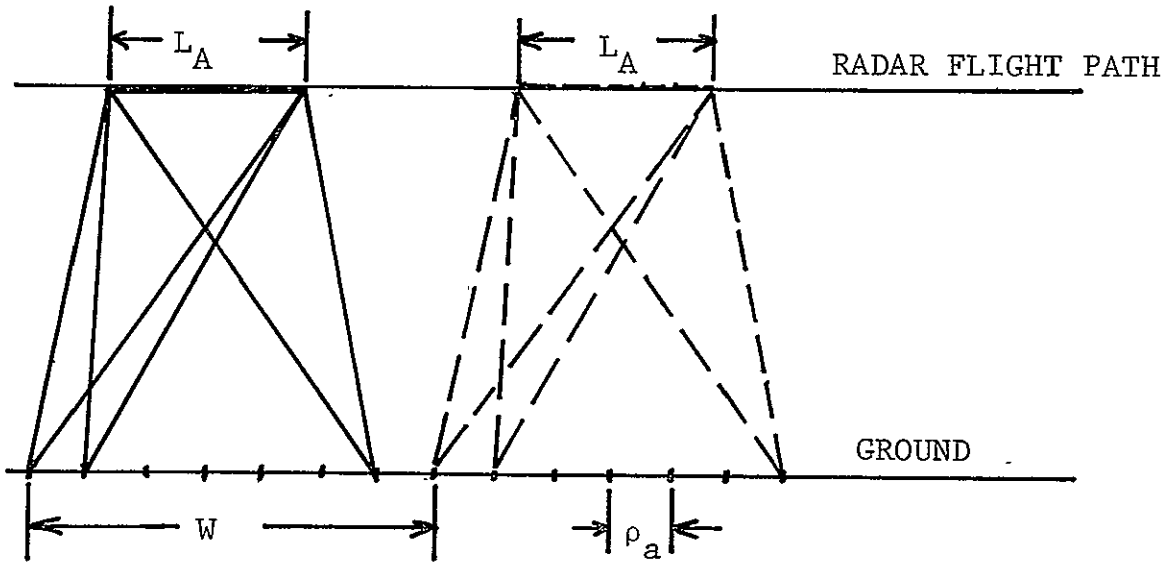

Figure 6-2. Batch Processing with Nonoverlapping Apertures

Note that the minimum PRF required to satisfy the azimuth ambiguity constaints is determined by the radar antenna. For a Venus Mapper mission, an antenna aperture of the order of 2 to 3 meters is assumed. Eq. (43) demonstrates that this will require a spatial sampling interval on the order of 1 meter. The desired azimuth resolution is on the order of 100 meters. Thus, presumming can result in a 100 to 1 reduction in data rate to the azimuth processor.

Continuous processing can only be conveniently accomplished for broadside mapping ($\theta_o = 90^o$). This is the normal mode for current airborne SAR's using coherent optical processors. It is an efficient method when all of the available Doppler bandwidth is used to obtain an azimuth resolution less than the antenna aperture. However, when much coarser resolution is acceptable, such as a Venus mapping mission, the batch mode of processing can result in a much more efficient radar system.

6.3 BATCH PROCESSING

In the batch processing mode, several azimuth image elements are generated at each range interval each time the radar moves a distance equal to the synthetic array length, as illustrated in Figure 6-2. In this mode, the required radar spatial sampling interval is finer than the azimuth resolution and is determined by the angular extent of the scene. Batch processing enables all points illuminated by the radar during the synthetic array interval to be

processed. Then, if the synthetic array length L_A is less than the azimuth extent of the illuminated patch W, the processing apertures are non-overlapping. This means that the radar can be turned off between processing intervals, thus conserving power without sacrificing SNR or resolution.

Batch processing can be used when mapping away from broadside and, hence, is more flexible than continuous processing. It can also make efficient use of fast Fourier transform processing algorithms that are easily matched to the phase modulation induced by the Doppler signal history.

6.4 DATA RATES

The required raw video sampling rate is equal to twice the RF bandwidth, or

$$R_V = 2B \tag{54}$$

The length of the video return is

$$T = \frac{2\Delta R}{c} \tag{55}$$

where ΔR is the mapped slant range target depth. From ambiguity constraints, this must be less than the pulse repetition interval. By buffering the sampled video, the signal can be stretched to fill the entire interpulse period. Then the average video data rate becomes

$$R_B = 2B \cdot T \cdot PRF$$

$$= 2B \cdot \frac{2\Delta R}{c} \cdot PRF$$

$$= \frac{2\Delta R}{\rho_r} \cdot PRF \qquad (56)$$

The minimum PRF is determined from ambiguity constraints given in Section 4. However, an additional data rate reduction can be obtained by presumming for continuous line-by-line processing; or by azimuth data buffering for batch processing.

For continuous processing the azimuth data can be low-pass filtered to a Doppler bandwidth of

$$B_D = \frac{V_N}{\rho_a} \qquad (57)$$

This corresponds to the minimum PRF if range offset or complex video is used. Then the minimum data rate is

$$R_{min} = \frac{2\Delta R}{\rho_r} \cdot B_D$$

$$= \frac{2\ \Delta R\ V_N}{\rho_r \rho_a} \qquad (58)$$

which is equal to twice the number of resolution cells mapped per unit time.

For batch processing, we recognize that the illuminated azimuth patch is much greater than the required synthetic aperture length if a partially focused synthetic aperture is used. The illuminated patch width is

$$W = \frac{R\lambda}{d_a} \qquad (59)$$

The required synthetic aperture length is

$$L_A = \frac{R\lambda}{2\rho_a} \qquad (60)$$

Then to map the azimuth patch given by Eq. (59), the radar data need only be collected for the distance given by Eq. (60). This results in an average data rate of

$$R_{AVE} = \frac{2\Delta R}{\rho_r} \cdot PRF \cdot \frac{L_A}{W}$$

$$= \frac{\Delta R}{\rho_r \rho_a} \cdot PRF \cdot d_a \qquad (61)$$

Substituting Eq. (43) for the minimum PRF, we get the result

$$R_{min} = \frac{2.7\ \Delta R\ V_N}{\rho_r \rho_a} \qquad (62)$$

By including Doppler prefiltering, the mapped azimuth swath W and the Doppler bandwidth are both reduced, and the numerical factor of 2.7 in Eq. (62) can be reduced to 2.0, as it is in Eq. (58).

7
ELLIPTICAL ORBIT CONSIDERATIONS

7.1 INTRODUCTION

The simplest analytical approach to planetary radar mapping is to consider a circular orbit, which results in essentially the same design equations and well known processing concepts that apply to the straight flight path aircraft case. When mapping from an elliptical orbit, the radar system must compensate for changing altitude and radial velocity. An additional consequence is the change in grazing angle due to changes in slant range when mapping with fixed squint and depression angles. Several reasonable mapping strategies for SAR operation in an elliptical orbit are given in Refs. [3 and 4]. Some of the results of these studies are reviewed here.

7.2 RESOLUTION

Since attainable azimuth resolution is independent of range, a 3-axis stabilized spacecraft can achieve the same resolution in an elliptical or circular orbit. However, since the required synthetic aperture length and azimuth compression ratio is proportional to range, processing complexity is increased. However, by preprocessing the data on board the spacecraft, the data link requirements are essentially unchanged.

7.3 AMBIGUITY CONSTRAINTS

The PRF and azimuth aperture constraints for an elliptical orbit are only slightly affected by the small changes in

velocity and squint angle. However, the range ambiguity and elevation aperture constraint are significantly affected by increasing range and decreasing grazing angle. To obtain adequate coverage at periapsis while satisfying ambiguity constraints at radar locations away from periapsis, a multi-beamwidth elevation antenna pattern may be required.

7.4 POWER REQUIREMENT

From Eq. (50), the average power requirements are proportional to the cube of slant range. Hence, for highly elliptical orbits, SNR may limit coverage away from periapsis. For the backscatter model given by Eq. (51), the decrease in σ_o with decreasing grazing angle for certain mapping strategies may also limit coverage due to inadequate SNR.

7.5 DATA PROCESSING

Due to the continuously changing range and the necessity for frequent alterations in the PRF required to prevent transmit-receive interference when mapping from an elliptical orbit, a perpetual line-by-line mode of processing may not be feasible. However, it has been shown [4] that a batch mode processor can easily be used, and in fact, is also recommended for circular orbit mapping. Hence, data processing does not have a significant impact on orbit selection.

8
SPINNING SPACECRAFT CONSIDERATIONS

8.1 INTRODUCTION

When mapping from a spin-stabilized spacecraft, the illuminated patch and available synthetic aperture length are restricted by the scanning motion of the antenna rather than by the orbital motion of the spacecraft. Depending on spin axis orientation and antenna mounting angle, this may significantly restrict coverage and/or resolution.

8.2 RESOLUTION

We will first consider a simplified geometry in which the spin axis is normal to both the radar velocity vector and the instantaneous antenna boresight direction. This is illustrated in Figure 8-1.

Let θ_T be the instantaneous angle between the velocity vector and a point target at range R. Let θ_p be the instantaneous angle between the velocity vector and the antenna boresight. Let time be referred to the center of the synthetic aperture at which time $\theta_p(0) = \theta_T(0)$. Then the antenna boresight direction during the synthetic aperture interval is

$$\theta_p(t) = \theta_p(0) + \Omega_p t \qquad (63)$$

where Ω_p is the antenna or spacecraft spin rate in rad/sec.

(Spin Axis Normal to Page)

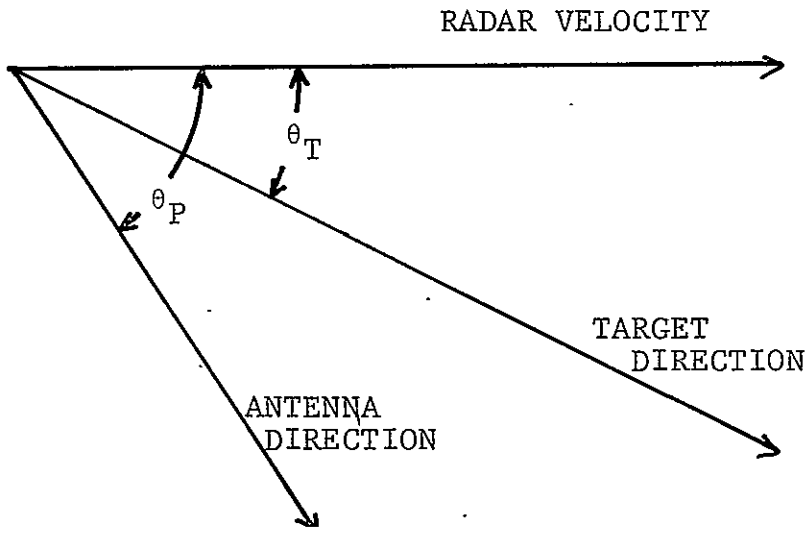

Figure 8-1. Planar Synthetic Array Geometry for a Spinning Spacecraft.

During the same interval, the angle to the target is given by the two-term Taylor Series expansion:

$$\theta_T(t) = \theta_T(0) + \Omega_T\, t \tag{64}$$

where

$$\Omega_T = \dot{\theta}_T(0) = \frac{V \sin \theta}{R} \tag{65}$$

is the instantaneous rotation rate of the target line-of-sight at the center of the synthetic aperture. Then, the total synthetic aperture length is determined by the length of time the target is within the antenna beamwidth β_a. This is given implicity by

$$\int_{-T_A/2}^{T_A/2} |\Omega_T - \Omega_P|\, dt = \beta_a \tag{66}$$

or, approximately, if the beamwidth is small by

$$T_A = \frac{\beta_a}{|\Omega_P - \Omega_T|} \tag{67}$$

Then the synthetic aperture length is

$$L_A = V\ T_A$$

$$= \frac{V\ \beta_a}{|\Omega_P - \Omega_T|} \tag{68}$$

Then from Eq. (33), the azimuth resolution is

$$\rho_a = \frac{R\lambda|\Omega_P - \Omega_T|}{2\ V\beta_a \sin\theta_o}$$

$$= \frac{\lambda}{2\ \beta_a} \frac{|\Omega_P - \Omega_T|}{|\Omega_T|}$$

$$= \rho_o \frac{|\Omega_P - \Omega_T|}{|\Omega_T|} \tag{69}$$

where

$$\rho_o = \frac{\lambda}{2\beta_a} \tag{70}$$

is the azimuth resolution attainable in the absence of antenna scanning.

In general, $\Omega_P >> \Omega_T$, then

$$\rho_a = \frac{\lambda R}{2\beta_a} \frac{\Omega_P}{V \sin \theta_o}$$

$$= \frac{R\, d_a}{2} \frac{\Omega_P}{V \sin \theta_o} \qquad (71)$$

and, hence, azimuth resolution is proportional to range, aperture size and rotation rate, and inversely proportional to radar velocity.

For the general case of nonplanar geometry, the respective angular rates are given by

$$\vec{\Omega}_P = \frac{\vec{S} \times \vec{R}}{R} \qquad (72)$$

and

$$\vec{\Omega}_T = \frac{\vec{V} \times \vec{R}}{R^2} \qquad (73)$$

where $\vec{S}$ is the spin vector, $\vec{R}$ is the instantaneous antenna boresight, $\vec{V}$ is the radar velocity vector, and $R = |\vec{R}|$ is the slant range.

8.3 AMBIGUITY CONSTRAINTS

The radar ambiguity constraints are determined by the instantaneous boresight direction, slant range and grazing angle and are given in Section 4. The most significant factor affecting the radar ambiguity constraint is grazing angle which changes rapidly during the antenna scan cycle. Thus, coverage may be limited by ambiguity constraints.

8.4 POWER REQUIREMENT

SNR and power requirements are independent of azimuth resolution and are given by Eq. (50) which applies to the spinning or boresight stabilized spacecraft. However, the average power in Eq. (50) represents the transmitter power averaged over one pulse repetition interval. When mapping from a spinning spacecraft, the radar transmitter can be turned off during the interval in which the ground is not illuminated or the ambiguity constraints cannot be satisfied. For the parameters considered in this study, the radar will be on for about 0.1 seconds over a 12 second spin cycle. Hence, the prime power requirements may be much less than predicted from Eq. (50).

8.5 DATA PROCESSING

Because the data is collected in bursts, a batch mode processing will be required. On-board processing will be

limited to Doppler tracking, which will be required to compensate for the change in instantaneous Doppler center frequency due to antenna scanning and spacecraft radial velocity, and PRF buffering.

The required data rates and data volume depend on orbit eccentricity and spin parameters. However, an estimate of the data handling requirements can be made by assuming the following nominal parameters:

Wavelength:	$\lambda = 10$ cm
RF Bandwidth:	$B = 3$ MHz
Grazing Angle:	$\psi = 78^{o}$
Slant Range:	$R = 1000$ km
Velocity:	$V_N = 6$ km/sec
Antenna Diameter:	$d = 2$ m
Spin Rate:	$S = 5$ rpm
Mapping Interval:	$T_M = 120$ msec
Quantization:	$q = 6$ bits
Returned data length:	$T = 70$ μsec

Then from Eq. (54), the nominal sampling rate is 6 MHz; from Eq. (45), the nominal two-way echo delay of the video return is 70 μsec; and from Eq. (43), the nominal PRF is 8 kHz. Then from Eq. (56), the buffered data rate is 3.4 MHz.

The spin period is 12 seconds. The video data is received for 120 msec. Hence, the average data rate over the spin cycle is approximately 30 kHz. This is the telemetry rate required to transmit the data in real time. For 6 bit quantization, the telemetry data rate is approximately 180 kbps. The PRF buffer storage is

$$N_{PRF} = 2\ B \cdot T \cdot q$$
$$\simeq 3 \text{ kbits} \qquad (74)$$

The total buffer storage for a spin cycle is

$$N_B = N_{PRF} \cdot PRF \cdot T_M$$
$$\simeq 3 \text{ Mbits} \qquad (75)$$

Azimuth correlation would be done with a ground based digital processor. Range pulse compression would be done either in the spacecraft or the ground processor.

9 COMPARISON OF THREE-AXIS STABILIZED SPACECRAFT AND SPINNING SPACECRAFT IMAGING CAPABILITIES

9.1 INTRODUCTION

Mapping from a spinning spacecraft represents a radical departure from conventional SAR techniques. However, if the required azimuth resolution is considerably coarser than the real-antenna azimuth aperture, then a short synthetic aperture time is required to obtain that resolution. If the spacecraft spin rate is slow enough to permit illumination of a target patch for the required interval, then a spinning spacecraft can provide the required resolution at the same power levels as a 3-axis stabilized spacecraft.

9.2 RESOLUTION

For a 3-axis stabilized spacecraft, the limiting azimuth resolution is equal to half the antenna aperture, and is independent of range, velocity and wavelength. For a spinning spacecraft and a narrow antenna beam, the azimuth resolution is given by

$$\rho_a = \frac{d}{2} \frac{|\vec{\Omega}_P - \vec{\Omega}_T|}{|\vec{\Omega}_T|} \qquad (76)$$

where d is the antenna diameter, $\vec{\Omega}_P$ is the instantaneous angular velocity of the antenna boresight, and $\vec{\Omega}_T$ is the rotation rate of the line-of-sight between the radar and a target. For the cases of interest, $|\vec{\Omega}_P| >> |\vec{\Omega}_T|$, then

$$\rho_a \simeq \frac{d}{2} \frac{|\vec{\Omega}_P|}{|\vec{\Omega}_T|}$$

$$\simeq \frac{d}{2} \frac{R\ S \sin \theta_m}{V_N} \tag{77}$$

where

$$|\vec{\Omega}_P| = S \sin \theta_m \tag{78}$$

$$|\vec{\Omega}_T| = \frac{V_N}{R} \tag{79}$$

and S is the spacecraft spin rate, θ_m is the mounting angle (half cone angle) between the antenna boresight and the spin axis, V_N is the radar velocity component normal to this instantaneous boresight direction, and R is the slant range to the illuminated target.

9.3 AMBIGUITY CONSTRAINTS

PRF ambiguity constraints are a function of antenna size, slant range, and instantaneous squint and grazing angles. For a 3-axis stabilized spacecraft in an elliptical orbit the squint and grazing angles are either controlled or slowly varying parameters, and any resulting ambiguity constraints tend to limit the angular mapping distance from periapsis.

For a spinning spacecraft, the grazing angle changes rapidly during the spin angle, and ambiguity constraints limit the coverage during a spin cycle. The result is that mapping will then be confined to that portion of the antenna scan which is closest to the spacecraft ground track. As a result, the operating duty cycle of the radar will be on the order of the antenna beamwidth divided by 2π.

9.4 POWER REQUIREMENTS

Power requirements for a specified range resolution, SNR, wavelength, orbital parameters, and terrain backscatter coefficients are a function of effective antenna aperture area only, as given in Eq. (50). Required antenna size is similar for the two cases. Hence, the scanning motion of the antenna is irrelevant with regard to power requirements or SNR.

9.5 DATA PROCESSING

Continuous or line-by-line processing can be used for the 3-axis stabilized spacecraft. Batch processing is required for the spin stabilized spacecraft. Since batch mode processing can be more efficient for coarse resolution radars, it may be preferred even for the 3-axis stabilized spacecraft in a circular orbit. Processing details for the spinning spacecraft are less conventional, and should be examined in more detail, yet no new techniques are required that are not already in use for other coherent pulsed Doppler radars.

10
RECOMMENDED SPIN PARAMETERS

10.1 INTRODUCTION

The principle parameters affecting the coverage pattern are the spin axis orientation at periapsis and the antenna boresight mounting angle with respect to the spin axis. Spin rate and antenna diameter affect swath width, resolution, and power requirements according to previously given equations.

The rectangular, planet-centered, coordinate system used in this study is shown in Figure 10-1. The positive z-axis is in the direction of periapsis, the positive x-axis is parallel to the spacecraft velocity vector at periapsis, and the y-axis is normal to the orbit plane.

The spin vector is defined by its magnitude, the angle θ_s between the spin vector and the orbit plane, and the angle ϕ_s between the spacecraft radius vector at periapsis and the projection of the spin vector on the orbit plane. The angle θ_s is positive when the y-component of spin is negative and ϕ_s is measured from the negative z axis in the clockwise direction as shown in Figure 10-1.

10.2 EFFECT OF ϕ_s

To simplify the argument, let us first consider a circular orbit. Given a fixed value of θ_s, an antenna mounting angle θ_m with respect to the spin axis, and ϕ_s, the intersection of the antenna line of sight with the planet surface will define some track. Along this track,

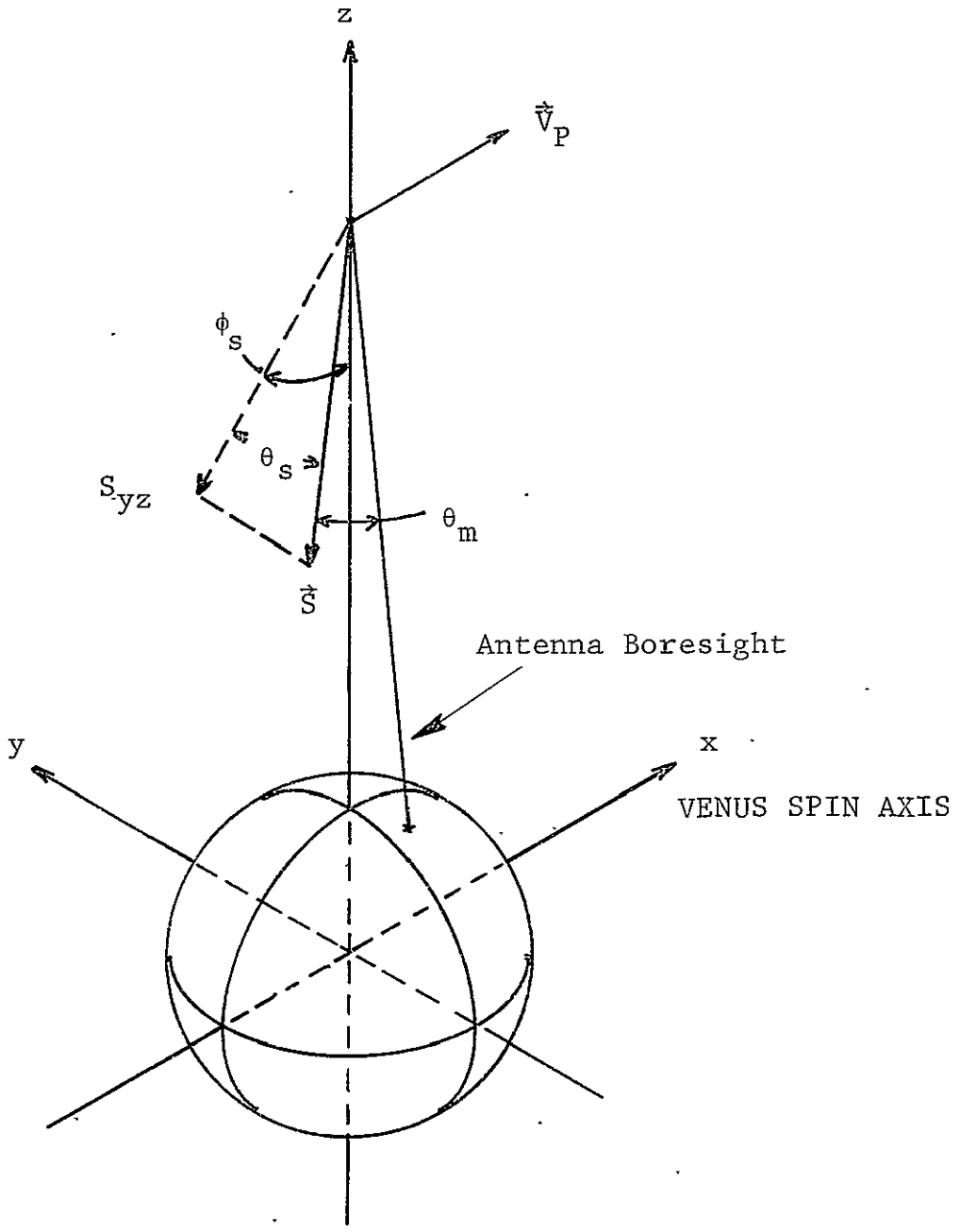

Figure 10-1. Coordinate System (at Periapsis)

the maximum grazing angle obtainable at a given position on the orbit occurs when the antenna axis, the spin vector, and the line from the radar to the center of the planet are all in the same plane. The peak grazing angle over the orbital period occurs when the component of the spin vector in the orbit plane points toward the center of the planet. For the case of $\dot{\phi}_s = 0$, the planet surface covered by the track is symmetric around periapsis. Since the spin axis is inertially fixed, the range to the mapped region will gradually increase, the maximum grazing angle will decrease and the contours bounding the mapping region will diverge as the spacecraft position departs from periapsis. Eventually the antenna boresight will completely miss the planet.

Values of ϕ_s other than zero will merely cause this same track to be shifted on the planet surface. The new track can be visualized by rotating all points of the track corresponding to $\phi_s = 0$ through an angle ϕ_s around the positive y-axis in Figure 10-1. Mapping parameters at a given point on the rotated track such as resolution, power, and so forth, will have the same values as those of the corresponding point on the $\phi_s = 0$ track. The surface coordinates of a point on the rotated track relate to those of the corresponding point on the $\phi_s = 0$ track by the matrix of axes rotations through an angle ϕ_s around the positive y-axis.

Based on the above discussion, the choice of ϕ_s mainly determines the region of coverage on the planet surface. The shape of this region and the mapping parameters are symmetric around the point of peak grazing angle.

The basic concept holds for elliptical orbits except that the vehicle altitude gradually increases from periapsis and the symmetry around the point of peak grazing angle.

is generally destroyed (except for $\phi_s = 0$ where the altitude changes symmetrically on either side of periapsis).

10.3 EFFECT OF θ_s

The combination of θ_s and θ_m determines the maximum grazing angle, the resolution and the shape of the antenna trace on the planet surface.

Neglecting the surface curvature, the peak grazing angle realized during the orbit equals the magnitude of the difference between θ_s and θ_m. This occurs when the component of the spin in the orbit plane points toward the center of the planet. The grazing angle is the single most important parameter that affects power requirements and the time-bandwidth product of the radar signal. Minimum power requirement is realized at the peak grazing angle because the highest radar cross section and the minimum range to the mapped region occur at maximum grazing angle.

The minimum time-bandwidth product also occurs at the peak grazing angle.

10.4 SIMULATION

A computer program was developed which calculates the mapping parameters, the power requirements, and the surface longitude and latitude of the target point for a given circular antenna aperture diameter, antenna mounting angle and a spin vector. A modified version of this program was developed which calculates the same parameters at the point of maximum grazing angle for each point on the orbit during the spin cycle.

The first version calculates the point-by-point parameters as the vehicle moves on orbit and the antenna spins around the spin axis. The modified version calculates the same parameters assuming the angular orientation of the antenna has been chosen such that the antenna is currently directed toward the maximum grazing direction at any point on orbit. The results obtained from the modified version clarify the effects of spin axis orientation and mounting angle on the mapping parameters. The percentage of coverage and the degree of overlap of the mappable region between consecutive cycles of spin are determined from the results of the original version.

Results of the modified simulations are given in the next three sections. For all cases, orbit eccentricity is 0.2, periapsis altitude is 500 km, antenna diameter is 2 meters, spin rate is 5 rpm, and the slant range resolution is 50 meters. Periapsis is assumed to be located at the equator. Azimuth resolution, time-bandwidth product and average transmitted power requirements for unity (0 dB)* SNR are plotted as a function of target latitude. Fixed radar parameters used for the power calculations are given in Section 5.

10.5 SPIN AXIS IN THE ORBIT PLANE

In this configuration, the spin axis is in the orbital plane, parallel to the planet surface at periapsis ($\phi_s = 90^o$, $\theta_s = 0^o$). This mode corresponds to the Pioneer Venus altimeter experiment which uses a continuously variable antenna mounting angle [5].

Figures 10-2 through 10-4 show resolution, time-band-

*This value is convenient for scaling although a nominal 10 dB is considered necessary for adequate radar opertion.

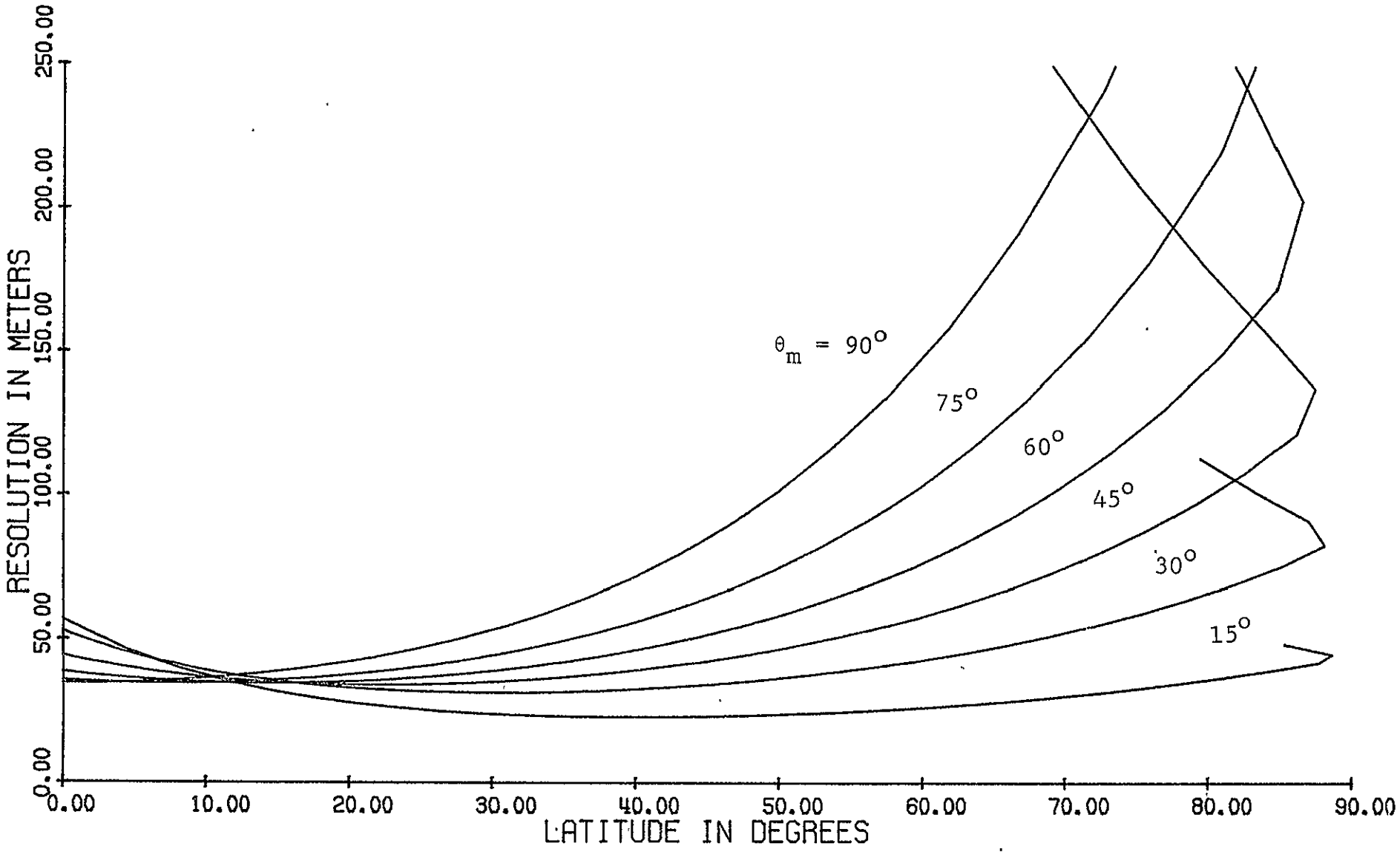

Figure 10-2. Resolution for Spin Axis in the Orbit Plane

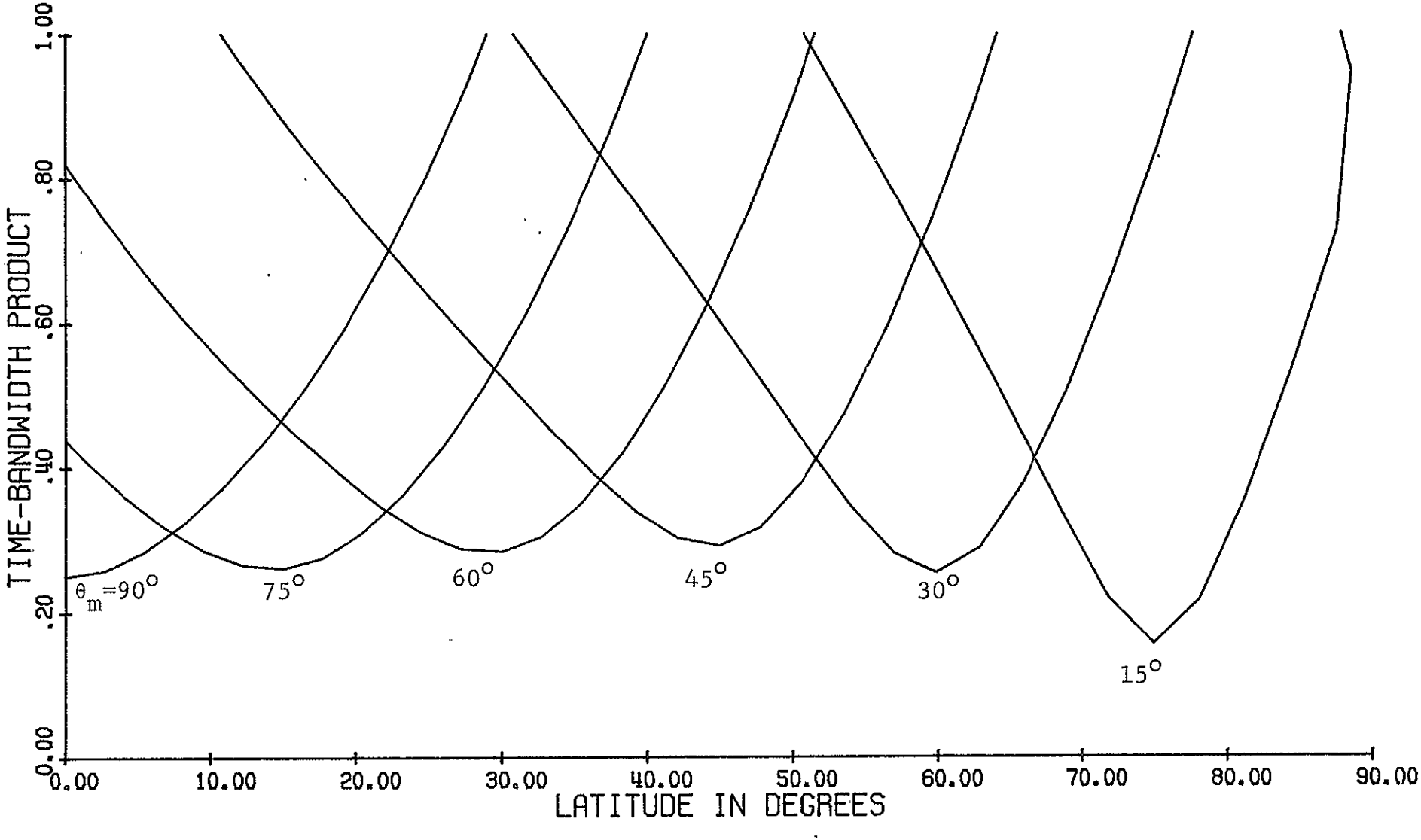

Figure 10-3. Time-Bandwidth Product for Spin Axis in the Orbit Plane.

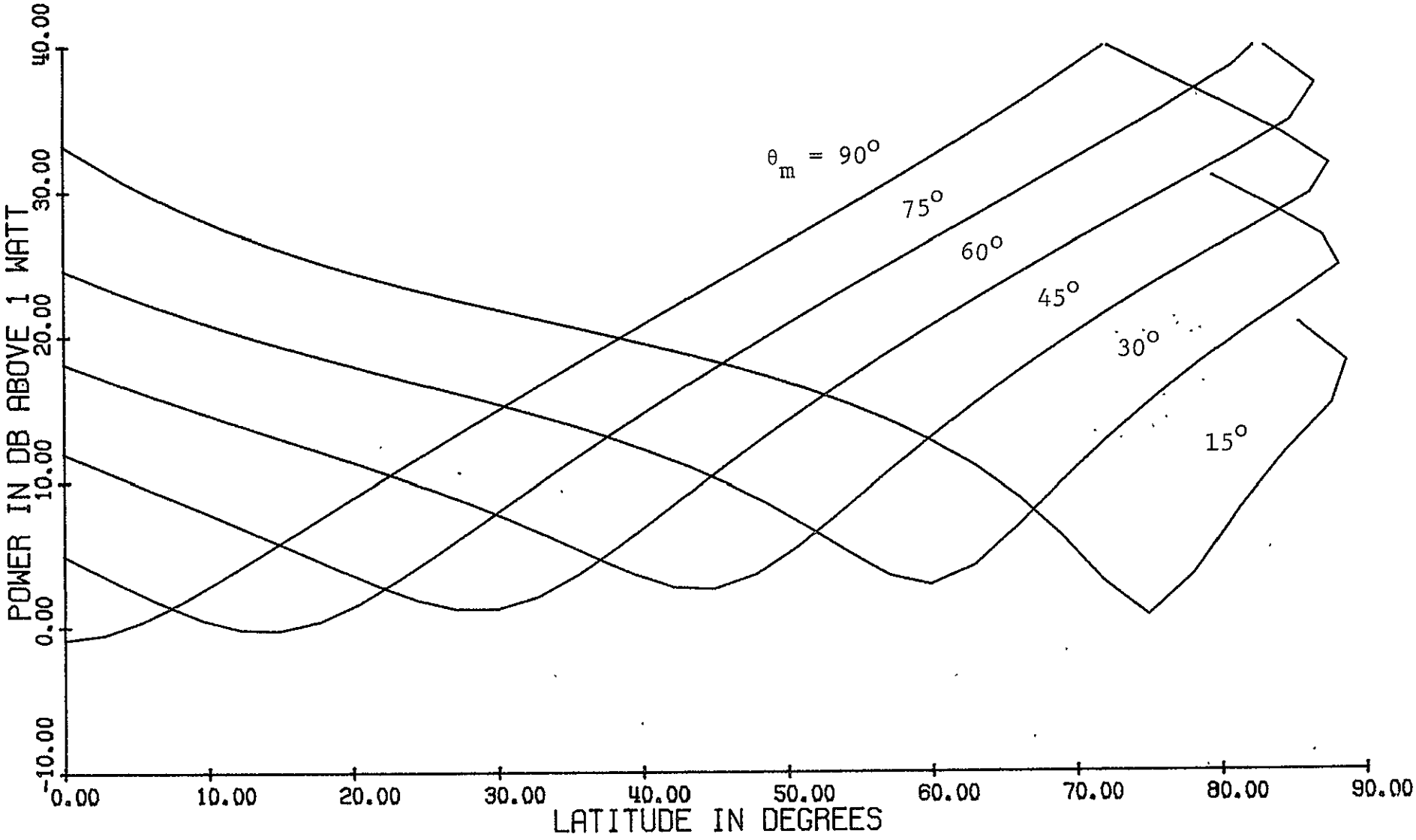

Figure 10-4. . Power Requirements for Spin Axis in the Orbit Plane.

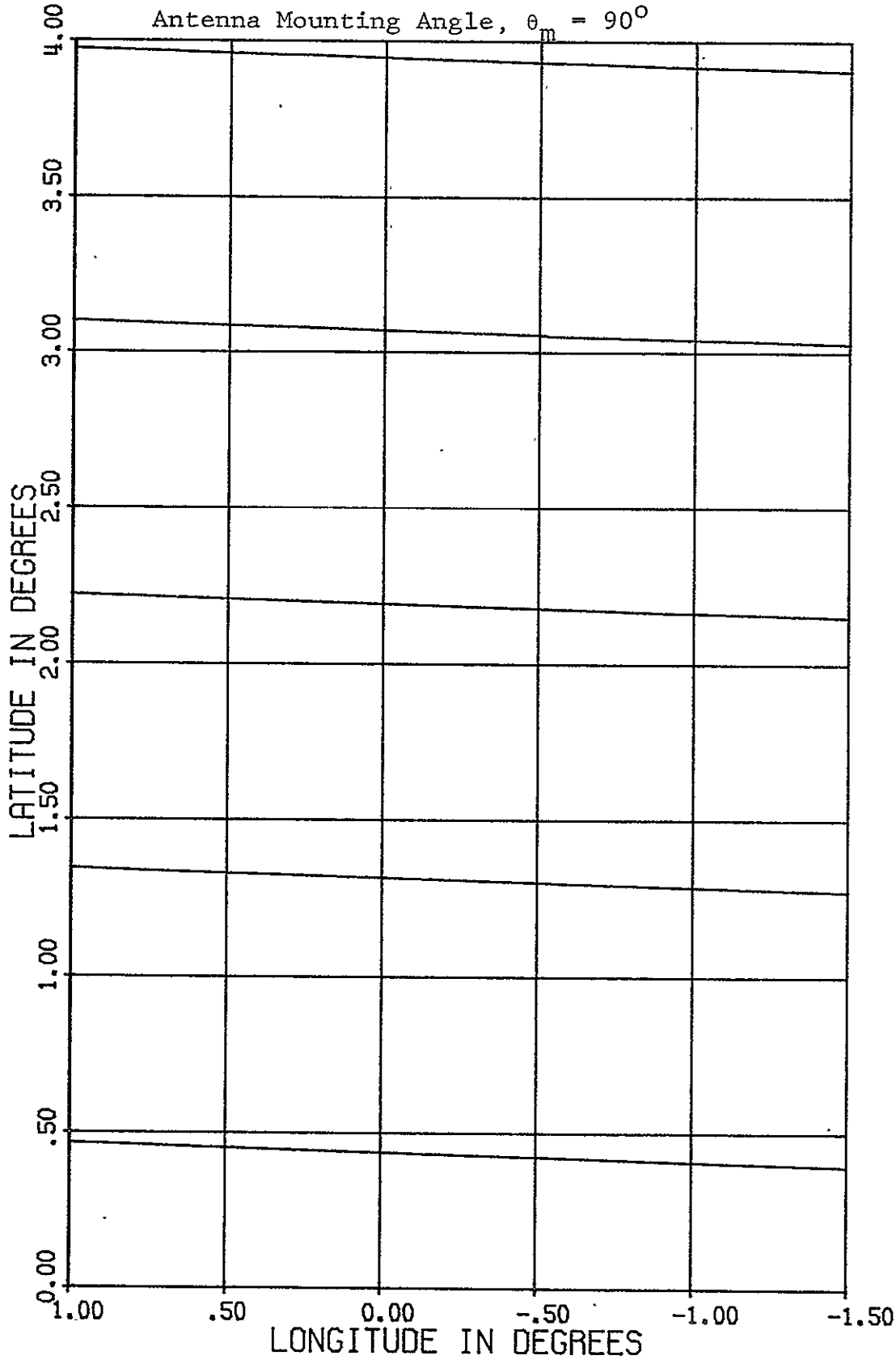

Figure 10-5. Ground Track for Spin Axis in the Orbit Plane.

width product and power requirements for different values of the antenna mounting angle θ_m. (Note that these curves reverse direction as the boresight passes over the point of maximum latitude.) The case of $\theta_m = 90^o$ results in symmetrical coverage about periapsis. As the mounting angle is decreased, higher latitudes are favored at the expense of the lower hemisphere. For a fixed antenna mounting angle, coverage is limited by ambiguity constraints (via the time-bandwidth product) and power requirements. However, if the antenna mounting angle can be changed continuously during the orbit, the resulting performance is given by the lower envelope of the curves shown in Figures 10-2 through 10-4.

Figure 10-5 shows the ground track of the antenna boresight near periapsis for a 90^o mounting angle. This represents the worst case coverage for a fixed antenna beamwidth. For the assumed 2 meter antenna, surface coverage is approximately 0.24 degrees of latitude or longitude at periapsis and steep grazing angles. Planet rotation is approximately 0.14 degrees longitude per orbit. Hence there is considerable cross-track overlap available if mapping is done on every orbit, but along-track coverage is inadequate. Since it does not seem practical to use successive orbits to fill the coverage gaps, this mode of operation does not seem useful.

10.6 SPIN AXIS NORMAL TO ORBIT PLANE

In this configuration, the spin axis is normal to the orbital plane and remains parallel to the planet surface at the nadir point during the entire orbit ($\theta_s = 90^o$). Coverage and power requirements are determined by the antenna mounting angle, which determines the grazing angle at the planet surface.

Figures 10-6 through 10-8 show resolution, time bandwidth product and power requirements for different values of antenna mounting angle. Note that for this case, all results are symmetric about periapsis.

Except for the fact that azimuth resolution is limited by the target dwell time, this case corresponds to a 3-axis stabilized spacecraft. In particular, ambiguity constraints and power requirements are identical for the two spacecraft.

Azimuth resolution is proportional to slant range, and hence varies only slightly with antenna mounting angle. However, time-bandwidth product and power requirements are very sensitive to grazing angle, and therefore vary significantly over small changes in mounting angle for angles near 80° (corresponding to a sidelook angle of 10° off nadir). In this case, improved performance might be achieved by incorporating a small ($\pm 5^{\circ}$) change in antenna mounting angle. This could improve coverage by operating at a shallower grazing angle at periapsis, and still permit adequate SNR by using a steeper grazing angle at higher latitudes.

Coverage for an antenna mounting angle of 80° is indicated in Figure 10-9. Only the portion of the spin cycle for which the time-bandwidth product is less than unity is shown. In this case cross-track coverage is approximately 0.2° plus 0.24° due to antenna beamwidth, or approximately three times the plant rotation interval per orbit. Figure 10-9 also indicates considerable overlap in the along-track direction. Since the illuminated patch size increases away from periapsis, this mode of operation can give complete planet coverage.

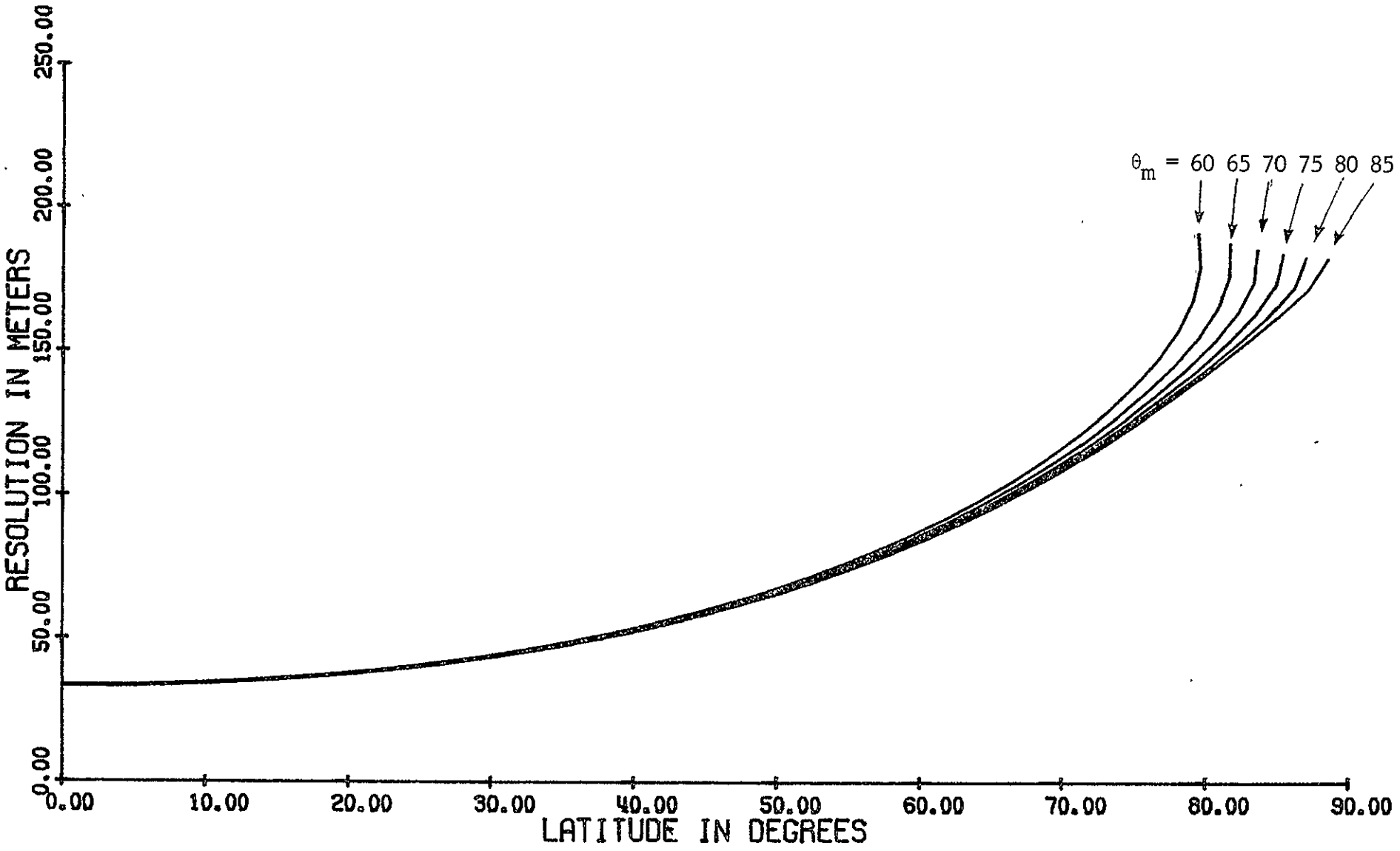

Figure 10-6. Resolution for Spin Axis Normal to the Orbit Plane.

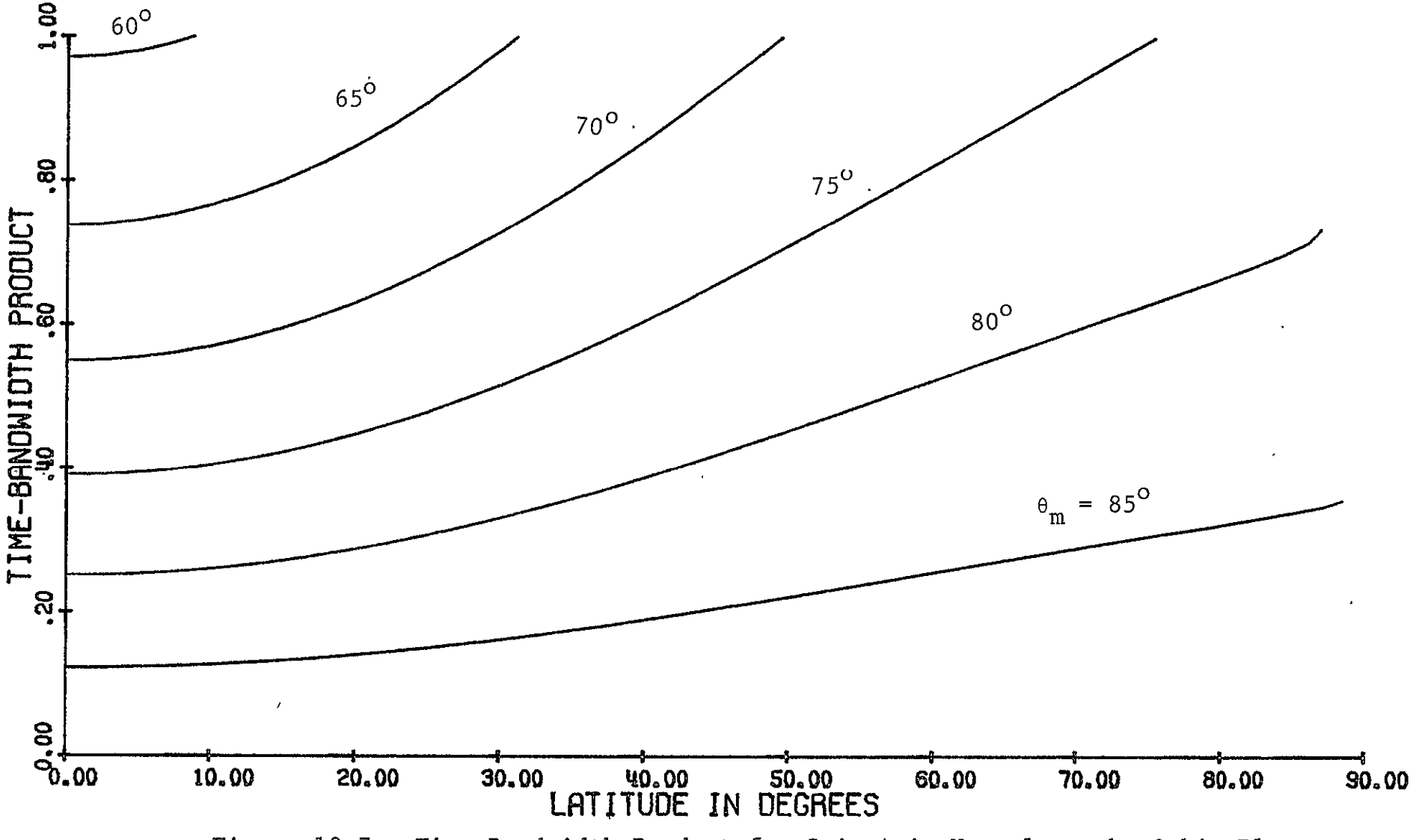

Figure 10.7. Time-Bandwidth Product for Spin Axis Normal to the Orbit Plane.

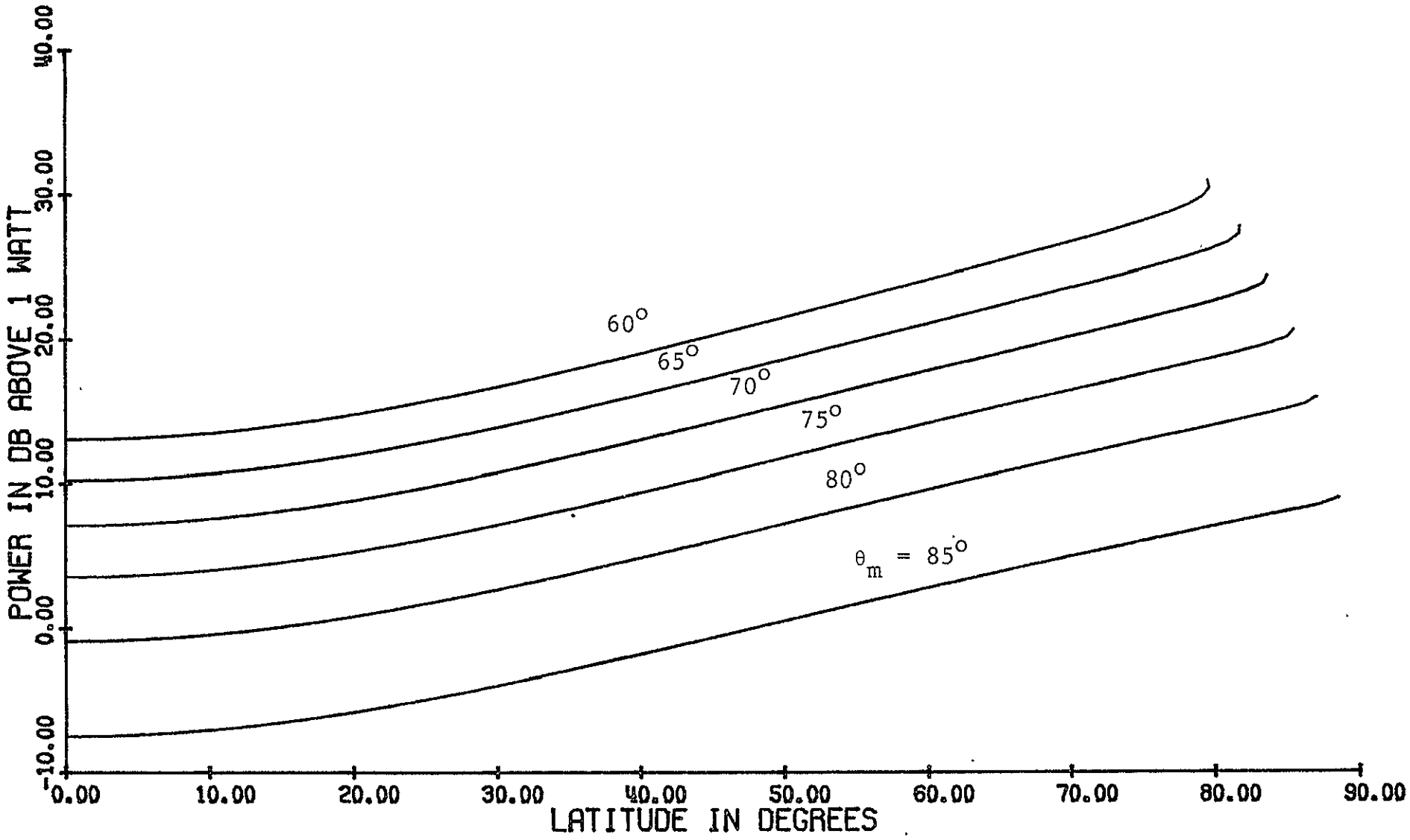

Figure 10-8. Power Requirement for Spin Axis Normal to the Orbit Plane

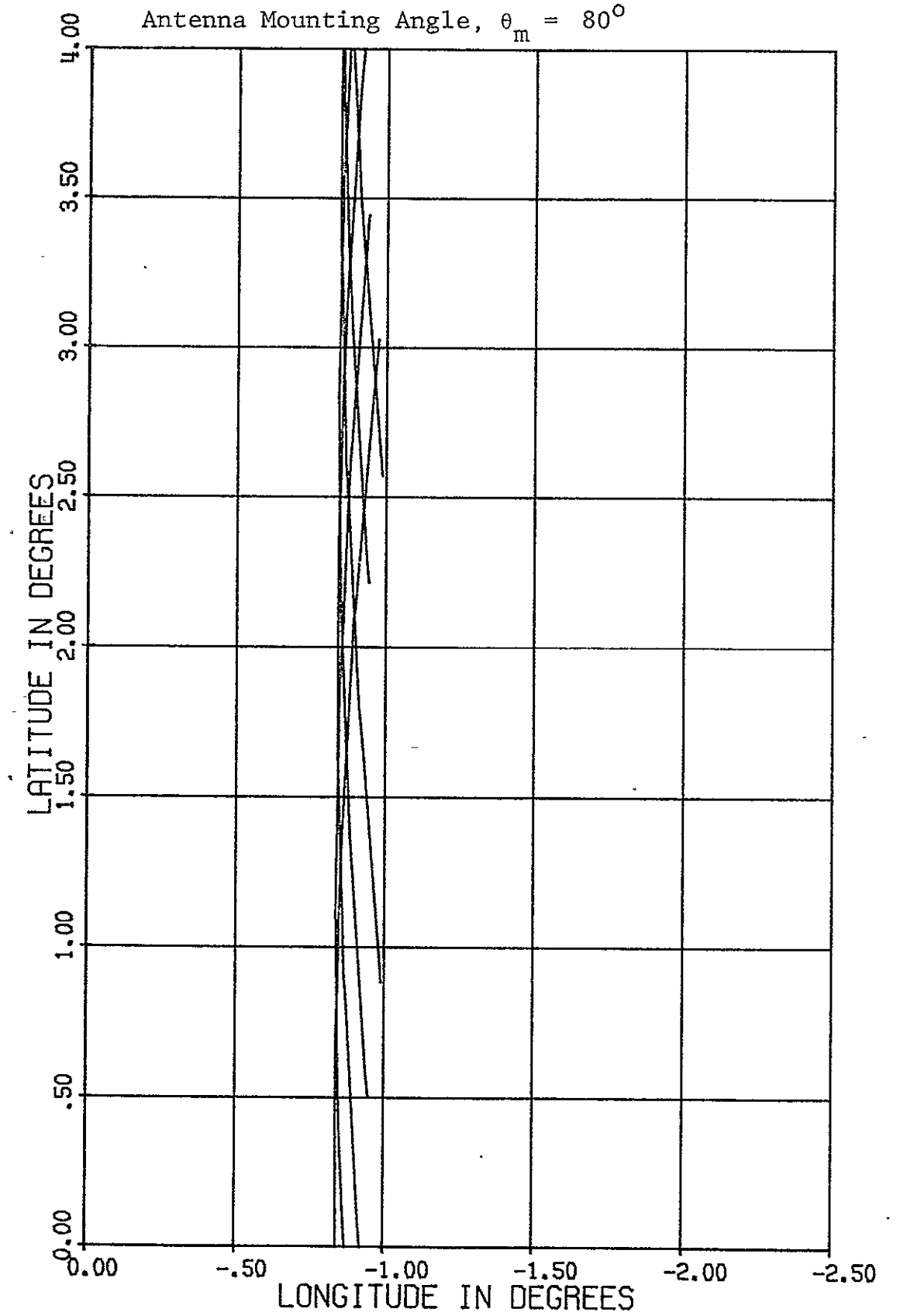

Figure 10-9. Ground Track for Spin Axis Normal to the Orbit Plane

10.7 GENERAL SPIN AXIS ORIENTATION

By orienting the spin axis just off the nadir point at periapsis and using a small antenna mounting angle, the ground track of the antenna boresight will trace a nominal spiral patch near the spacecraft ground track. As the antenna mounting angle approaches zero, the achievable azimuth resolution approaches half the antenna diameter. However, it is easy to show that this mode of operation will permit mapping only near periapsis since the grazing angle will decrease rapidly as the spacecraft departs from periapsis. This will quickly lead to a time-bandwidth product greater than unity which will render the system ambiguous.

Another approach to the general case is to consider a slight modification from mapping normal to the orbital plane. By decreasing the angle of the spin axis from the orbital plane, the spin component normal to the line-of-sight can be reduced, thus improving azimuth resolution. By increasing the angle ϕ_s from zero, the latitude corresponding to the peak grazing angle can be increased.

Figures 10-10 through 10-13 show results for a spin axis 15^o from the normal to the orbit plane ($\theta_s = 75^o$) and an antenna mounting angle of 65^o, with the orientation of the spin axis in the orbit plane (ϕ_s) as a parameter.

As ϕ_s is increased from 0^o (normal to planet surface at periapsis), the position of the peak grazing angle travels toward the planet pole, so does the position of minimum power and time-bandwidth product. The antenna mounting angle is 65^o from the spin axis, leaving a maximum possible grazing angle of 10^o.

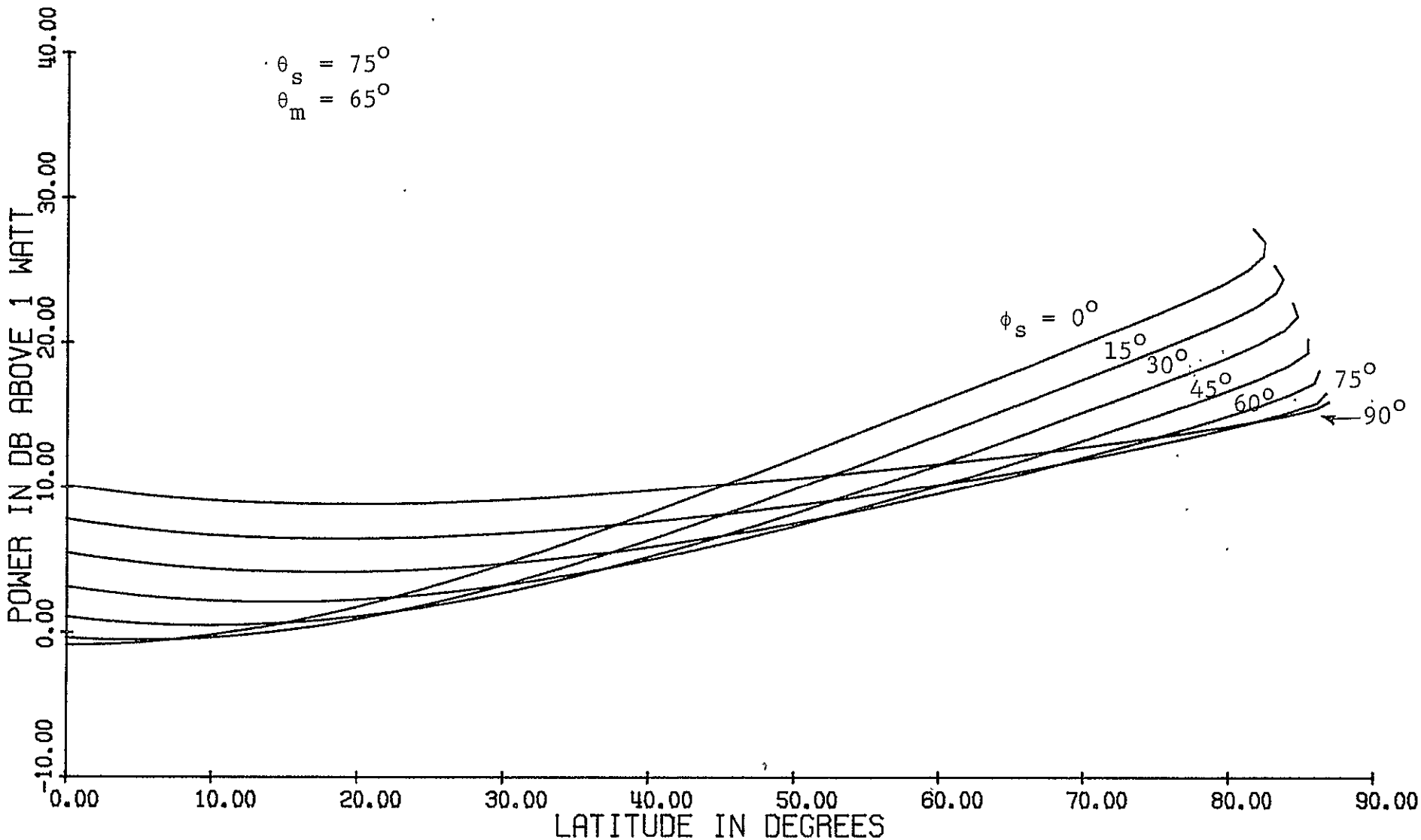

Figure 10-10. Resolution for General Spin Axis Orientation.

Figure 10-11. Time-Bandwidth Product for General Spin Axis Orientation

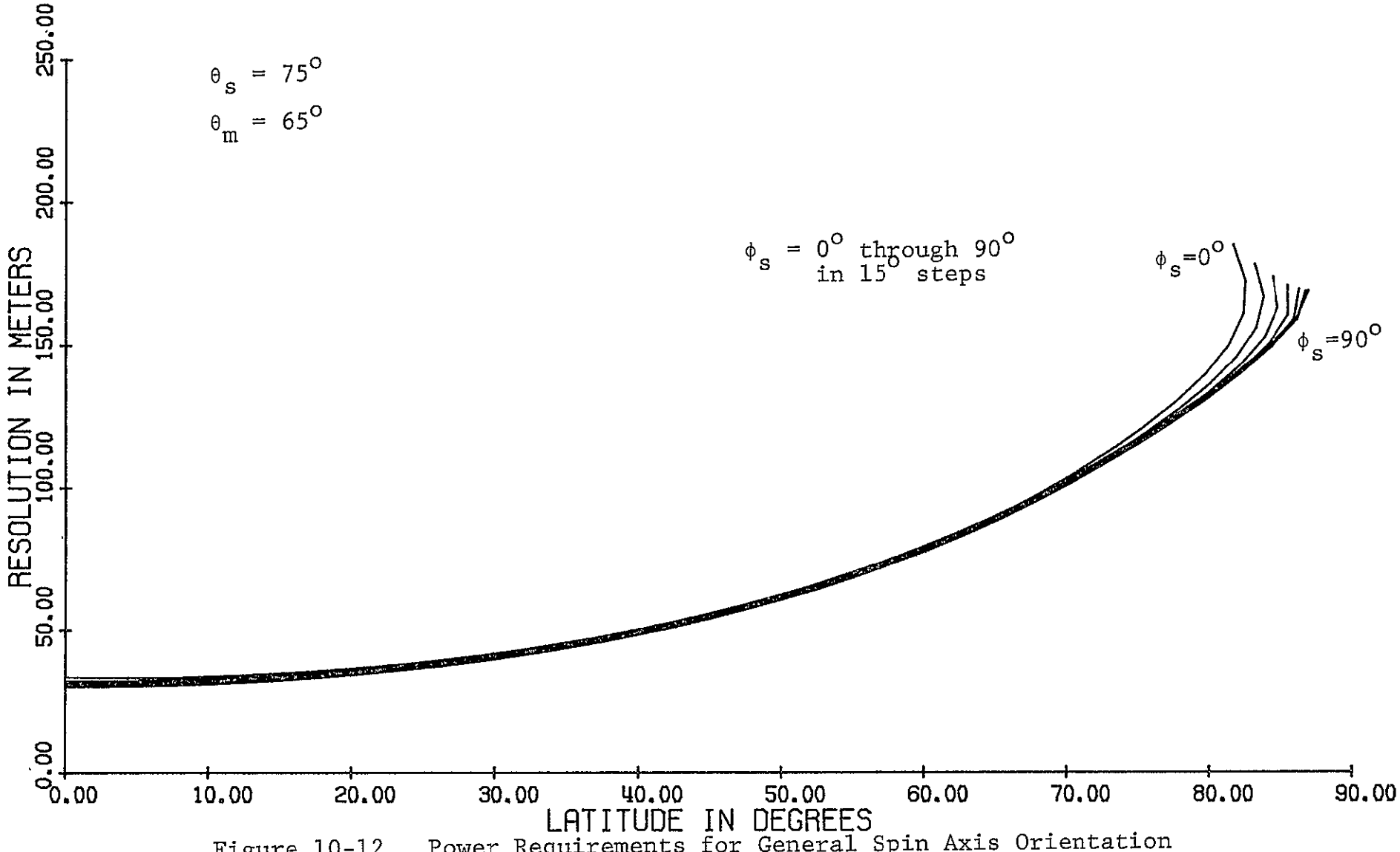

Figure 10-12. Power Requirements for General Spin Axis Orientation

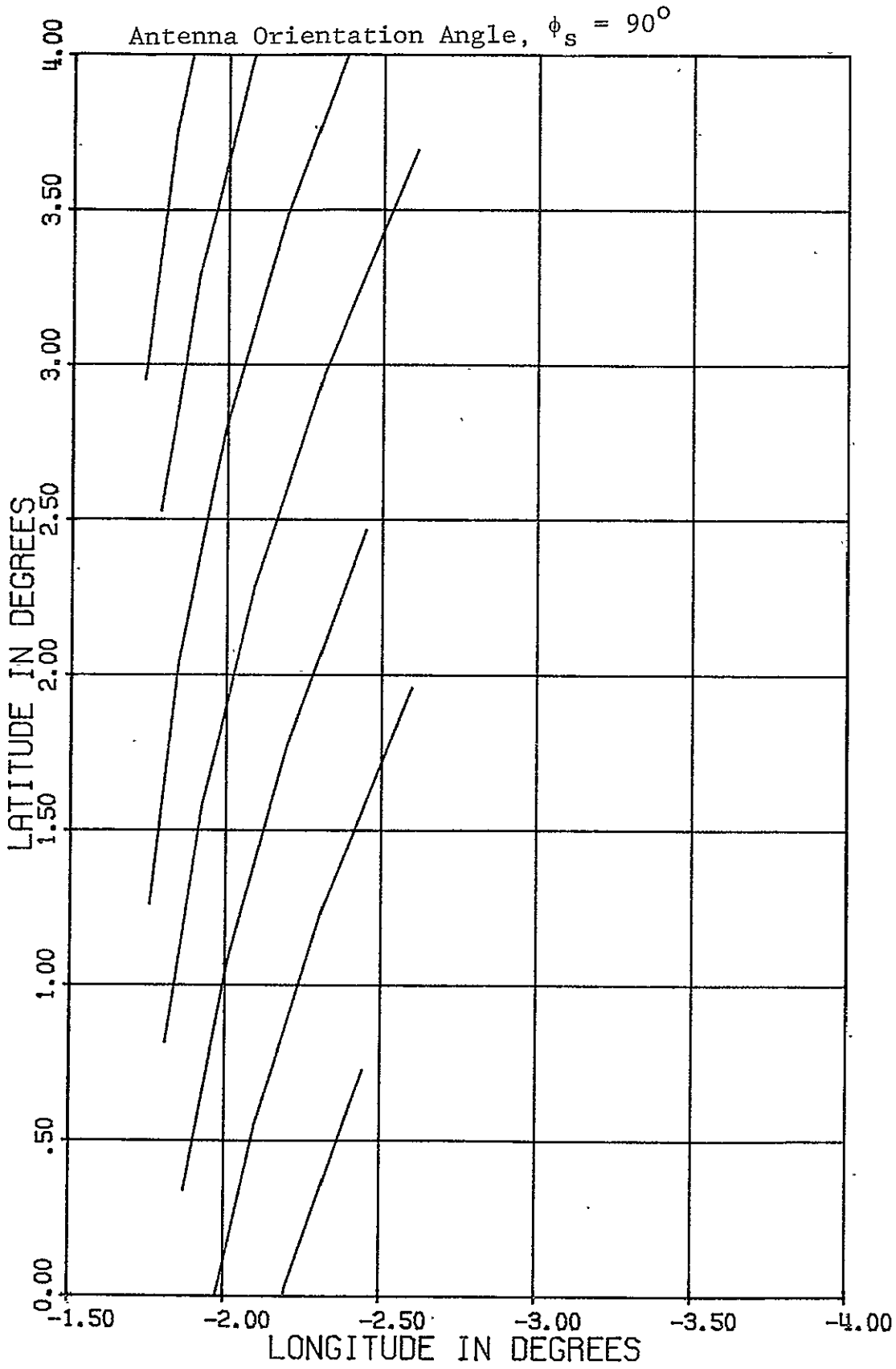

Figure 10-13. Ground Track for General Spin Axis Orientation

Comparing these graphs to Figures 10-6 through 10-8, we find that on the power and time-bandwidth product plots the curve corresponding to $\theta_s = 90^o$ and $\theta_m = 80^o$ forms the envelope to the minima on the corresponding curves for $\theta_s = 75^o$ and $\theta_m = 65^o$. This is expected since in all cases the maximum possible grazing angle is 80^o. In the case of the spin axis normal to orbit plane the spin component in the orbit plane is zero and there is no preferred orientation, that is, the maximum possible grazing angle can be realized at any point on the orbit. In contrast, when the spin axis is not normal to the orbit plane the peak grazing angle will occur when the component of the spin in the orbit plane points toward the center of the planet. This condition is met at only one point on the orbit. At other positions the grazing angle will have a local maximum less than 80^o. This coincides with the argument given above on the effect of θ_s.

Comparing the curves for resolution we find that some gain is achieved when the antenna is tilted from the normal to the orbit plane and the mounting angle is readjusted to realize the same maximum grazing angle. This is mainly due to the reduced component of the spin normal to the antenna axis as discussed in Section 10.3.

Figure 10-13 shows the ground track of the antenna boresight for $\theta_s = 75^o$ and $\phi_s = 90^o$. This orientation increases the cross-track coverage, but introduces some gaps in the along-track coverage near periapsis.

10.8 EFFECTS OF PARAMETER VARIATIONS

Figure 10-2 through 10-13 are based on an antenna diameter of 2 meters and a spin rate of 5 rpm. Some simple adjustments can be made for variations in these parameters.

Increasing antenna diameter by a factor, k, increases azimuth resolution cell size by k, decreases the time-bandwidth product by k^2 and decreases the power requirement by k^4. Increasing the spin rate by a factor, k, increases azimuth resolution cell size by k and leaves time-bandwidth product and power requirements unchanged. Coverage is affected by the corresponding changes in beamwidth and scan rate.

10.9 CONCLUSIONS

By placing the spin axis normal to the orbital plane and the antenna mounting angle such that the boresight is 10 to 15 degrees off nadir, complete planet coverage at 30 to 160 meter azimuth resolution is attainable. The average transmitter power required for a SNR of 10 dB is 10 to 200 watts during a nominal 120 msec mapping interval once per spin cycle. The average power over a 12 second spin cycle is 0.1 to 2 watts. By allowing a small adjustment in antenna mounting angle during the orbit, the surface grazing angle can be held constant at 72 to 78 degrees, thus providing a large value of backscatter coefficient, permitting mapping at reasonable average power levels.

11
EXTENSIONS

11.1 POST-DETECTION INTEGRATION

Results of the previous sections apply to single-look imagery. The mean intensity of the resulting imagery will correspond to the actual surface cross-section; however due to random phases of the terrain return, the variance of the image intensity will be equal to the mean, and will be independent from cell to cell. The result is the typical speckle pattern associated with coherent imaging systems.

If excess Rf or Doppler bandwidth is available, this speckle can be reduced by post-detection integration, in which the additional data is noncoherently added after linear or square law detection. This is generally refered to as mixed integration, or multi-look processing.

By averaging N independently obtained image samples corresponding to the same pixel, the image variance to mean square ratio is reduced to 1/N. Independent samples are obtained by either frequency diversity (increased RF bandwidth) or angle diversity (increased Doppler bandwidth). For a spinning spacecraft, diversity may be attained by using overlapping images gathered on successive spin cycles. This is a form of angle diversity.

In order to obtain an image intensity estimated with a standard deviation equal to 10 percent of the mean, 100 independent samples must be noncoherently averaged. For the case of a spinning spacecraft, only a few (less than 10) looks at any target area can be obtained when operating at the best available resolution. Additional noncoherent integration can be obtained only by sacrificing resolution. However, it

has not been shown that the resulting decrease in image variability offsets the loss in resolution. Hence, a minimal amount of noncoherent integration, determined by overlapping coverage, is likely to be attained.

11.2 STEREO

When mapping with the spin axis normal to the orbit plane, images from successive spin cycles may have a sufficient angular displacement to permit stereo viewing. At periapsis, the distance between image frames is approximately 100 km corresponding to an angular separation of about 11^{o} which corresponds to normal stereo viewing angles.

REFERENCES

1. MacKay, J.S., et al., "A Preliminary Analysis of a Radar Mapping Mission to Venus," NASA TM X-2868, September 1973.

2. Friedman, L.D. and S.R. Rose, "Venus Orbital Imaging Radar (VOIR) Study, Final Report," JPL Report No. 760-89, November 1973.

3. Scofield, W. T., D. B. Cross, et al., "A Study of an Orbital Radar Mapping Mission to Venus, Final Report," Martin-Marietta Aerospace, Denver Division, NASA CR-114640, 114641, and 114642, September 1973.

4. Scofield, W. T., D.B. Cross, et al., "Venus Orbital Imaging Radar (VOIR) Technical Tradeoffs Study," Final Report, Martin-Marietta Aerospace, Denver Division, Report No. MCR-74-276, August 1974.

5. "Pioneer Venus Orbiter Scientific Instrument-Radar Mapper," Pioneer Document PC-417, NASA Ames Research Center.

6. Larson, R. W., J. S. Zelenka and E. L. Johansen, "A Microwave Hologram Radar System," IEEE Transactions AES-8, pp. 208-217, 1972.

7. Larson, R. W., et al., "Investigation of Microwave Hologram Techniques for Application to Earth Resources," Proceedings of the Ninth International Symposium on Remote Sensing of Environment, pp. 1541-1569, 1974.

8. Bayma, R. W. and P.A. McInnes, "Aperture Size and Ambiguity Constraints for a Synthetic Aperture Radar," Proceedings of the IEEE International Radar Conference, pp. 499-504, 1975.

9. Mims, J.H. and J.L. Farrel, "Synthetic Aperture Imaging with Maneuvers," IEEE Transactions, AES-8, pp. 410-418, 1972.

10. Kirk, J.C., Jr., "A Discussion of Digital Processing in Synthetic Aperture Radar," IEEE Transactions, AES-11, pp. 326-337, 1975.

BIBLIOGRAPHY

Brown, W.M., "Synthetic Aperture Radar," IEEE Trans. Aerospace and Electronic Systems, vol. AES-3, pp. 217-229, March 1967.

Brown, W.M., and L.J. Procello, "An Introduction to Synthetic Aperture Theory," IEEE Spectrum, pp. 52-62, September, 1969.

Cutrona, L.J., W.E. Vivain, E.N. Leith, and G. O. Hall, "A High-resolution Radar Combat-surveillance System," IRE Trans. Military Electronics, vol. MIL-5, pp. 127-131, January 1961.

Cutrona, L.J. and G.O. Hall, "A Comparison of Techniques for achieving fine azimuth resolution," IRE Trans. Military Electronics, vol MIL-6, pp. 119-121, April 1962

Harger, R.O. Synthetic Aperture Radar Systems Theory and Design. New York: Academic Press, 1970.

Heimiller, R.C., "Theory and Evaluation of Gain Patterns of Synthetic Arrays," IRE Trans. Military Electronics, vol. MIL-6, pp. 122-130, April 1962.

Matthews, R.E. ed, Active Microwave Workshop Reports, NASA SP-376, 1975.

McCord, H. L., "The Equivalence among Three Approaches to Deriving Synthetic Array Patterns and Analyzing Processing Techniques," IRE Trans. Military Electronics, vol. MIL-6 pp. 116-119, April 1962.

Moore, R.K. et al, Microwave Remote Sensors; Chapter 9, Manual of Remote Sensing, Volume I, Janza, F.J. ed., American Society of Photogrammetry, Fails Church, Va. 1975.

Sherwin, C.W., J.P. Rauna, and R.D. Rawcliffe, "Some early Developments in Synthetic Aperture Radar Systems," IRE Trans. Military Electronics, vol. MIL-6, pp. 111-115, April 1962.

Skolnik, M.I., ed., Radar Handbook, McGraw-Hill, 1970.